HHS Public Access

Author manuscript

Cell Rep. Author manuscript; available in PMC 2025 April 19.

Published in final edited form as:

Cell Rep. 2025 March 25; 44(3): 115371. doi:10.1016/j.celrep.2025.115371.

RNF10 and RIOK3 facilitate 40S ribosomal subunit degradation upon 60S biogenesis disruption or amino acid starvation

Pierce W. Ford[1], **Danielle M. Garshott**[1,2], **Mythreyi Narasimhan**[1], **Xuezhen Ge**[1], **Eric M. Jordahl**[1], **Shubha Subramanya**[1], **Eric J. Bennett**[1,3,*]

[1]School of Biological Sciences, Department of Cell and Developmental Biology, University of California, San Diego, La Jolla, CA 92093, USA

[2]Present address: Department of Molecular and Cell Biology, University of California, Berkeley, Berkeley, CA, USA

[3]Lead contact

SUMMARY

The initiation-specific ribosome-associated quality control pathway (iRQC) is activated when translation initiation complexes fail to transition to elongation-competent 80S ribosomes. Upon iRQC activation, RNF10 ubiquitylates the 40S proteins uS3 and uS5, which leads to 40S decay. How iRQC is activated in the absence of pharmacological translation inhibitors and what mechanisms govern iRQC capacity and activity remain unanswered questions. Here, we demonstrate that altering 60S:40S stoichiometry by disrupting 60S biogenesis triggers iRQC activation and 40S decay. Depleting the critical scanning helicase eIF4A1 impairs 40S ubiquitylation and degradation, indicating mRNA engagement is required for iRQC. We show that amino acid starvation conditions also stimulate iRQC-dependent 40S decay. We identify RIOK3 as a crucial iRQC factor that interacts with ubiquitylated 40S subunits to mediate degradation. Both RNF10 and RIOK3 protein levels increase upon iRQC pathway activation, establishing a feedforward mechanism that regulates iRQC capacity and subsequent 40S decay.

Graphical Abstract

*Correspondence: e1bennett@ucsd.edu.

AUTHOR CONTRIBUTIONS

Conceptualization, D.M.G., P.W.F., and E.J.B.; methodology, D.M.G., P.W.F., X.G., and E.J.B.; validation, D.M.G., P.W.F., and X.G.; formal analysis, P.W.F. and E.J.B.; investigation, P.W.F., D.M.G., M.N., E.M.J., S.S., and X.G.; writing, P.W.F. and E.J.B.; visualization, P.W.F. and E.J.B.; supervision, E.J.B.; funding acquisition, E.J.B.

DECLARATION OF INTERESTS

E.J.B. receives research funding from Pfizer, Inc.

SUPPLEMENTAL INFORMATION

Supplemental information can be found online at https://doi.org/10.1016/j.celrep.2025.115371.

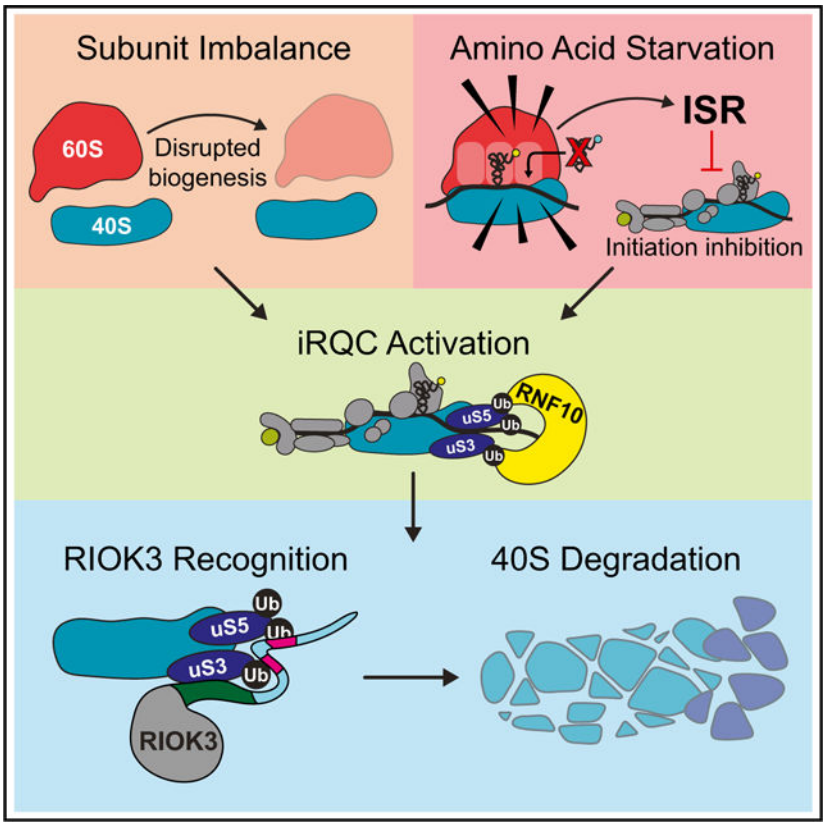

In brief

Ford et al. show that depleting 60S subunits and altering ribosomal stoichiometry activates the iRQC pathway. The ubiquitin-binding kinase RIOK3 is a new iRQC factor that facilitates 40S degradation. The iRQC pathway utilizes a feedforward mechanism of autoregulation where iRQC-stimulating conditions increase RNF10 and RIOK3 expression.

INTRODUCTION

Elaborate translation control mechanisms respond to highly dynamic and rapidly changing cellular conditions by tuning protein biosynthesis activity.[1] While most translation events culminate in functional protein synthesis, defects within mRNA transcripts, nascent chains, or ribosomes themselves can impede ribosome progression.[2–4] Distinct ribosome-associated quality control (RQC) pathways recognize, triage, and clear stalled ribosomal complexes, and sustained RQC engagement activates cellular stress pathways.[4–7]

Precise ubiquitylation of specific ribosomal proteins is a key step within diverse RQC-related pathways that allow for downstream ribosomal stall resolution.[5,8–14] Integrated stress response (ISR) activation or translation initiation inhibition results in the site-specific ubiquitylation of the 40S proteins uS3 (RPS3) and uS5 (RPS2).[15] These ubiquitylation events are regulated by the ubiquitin ligase RNF10 and the deubiquitylating enzyme USP10.[16–18] Sustained uS3 and uS5 ubiquitylation upon RNF10 overexpression or USP10 depletion results in autophagy-independent 40S destruction.[17] Despite the characterization

of this new initiation-specific branch of the RQC pathway (iRQC), cellular conditions that stimulate iRQC pathway activity in the absence of pharmacological inhibitors are unknown. The observation that USP10 depletion results in constitutive uS3 and uS5 ubiquitylation on up to 20% of all ribosomes in otherwise untreated cells suggests that the iRQC nucleating event occurs regularly during homeostatic cellular conditions.[16,17] Furthermore, the mechanisms that facilitate 40S degradation after initial RNF10-mediated ubiquitylation and the cellular factors that participate in this ribosomal triage pathway remain uncharacterized.

Ribosomes are elaborate ribonucleoproteins, and ribosome biogenesis is a carefully orchestrated process involving dozens of dedicated ribosome assembly factors.[19–22] Initial rRNA production, processing, and ribosomal protein incorporation steps occur in the nucleolus. Despite early steps that coordinate 60S and 40S production, 60S and 40S biogenesis largely occurs via distinct assembly pathways. The final subunit maturation and rRNA processing steps occur in the cytoplasm, culminating in the release and recycling of bound biogenesis factors and generation of translation-competent subunits.[21,22] Differences in individual subunit biogenesis pathway activity and function can lead to non-stoichiometric production of 60S or 40S subunits that may activate quality control pathways to restore normal stoichiometry.[23–32] Further, rRNA damage or inaccurate biosynthesis can result in the production of subunits that are unable to engage in the translation cycle with appropriate kinetics or fidelity. Quality control pathways would then be necessary to identify and target defective 40S ribosomal subunits that engage with mRNA and impair total translation capacity.

Pioneering research in S. cerevisiae characterized independent ribosome quality control pathways that catalyze the destruction of non-functional 18S and 25S rRNAs when incorporated into individual subunits.[33–35] These 18S and 25S non-functional rRNA decay (NRD) pathways require both active translation and distinct ubiquitin-pathway components to eliminate defective rRNA molecules.[34–37] 18S NRD requires Mag2 (*S. cerevisiae* RNF10 ortholog) to ubiquitylate uS3 on the same conserved uS3 lysine residue that is ubiquitylated by RNF10 in response to iRQC activation.[38] While there are some similarities with the mammalian iRQC pathway and the yeast 18S NRD pathway, the two pathways are activated by distinct agonists, and a mammalian 18S NRD pathway has not been described.

Here, we demonstrate that broad genetic disruption of 60S biogenesis results in enhanced RNF10-dependent uS3 and uS5 ubiquitylation and subsequent 40S degradation in human cells. The 40S decay observed upon impairing 60S biogenesis requires both RNF10 and the translation initiation factor eIF4A1, indicating that mRNA engagement and scanning by 43S preinitiation complexes are required for iRQC activity. We provide evidence that RNF10 protein levels increase upon 60S biogenesis disruption and define a translational control mechanism that regulates RNF10 protein abundance. We identify RIOK3 as the reader of uS3 and uS5 ubiquitylation and demonstrate that RIOK3 ubiquitin binding and kinase activities are required to facilitate 40S decay. We demonstrate that depletion of RIOK3 leads to an accumulation of ubiquitylated 40S ribosomes, indicating that RIOK3 acts downstream of RNF10 and that ribosome ubiquitylation itself is not sufficient for 40S degradation. Further, we show that amino acid starvation results in altered ribosomal

subunit stoichiometry driven by RIOK3- and RNF10-dependent 40S decay. Collectively, these results reveal that diverse biological conditions can stimulate iRQC-dependent 40S degradation and that iRQC capacity is regulated by a feedforward mechanism that elevates RNF10 and RIOK3 levels upon iRQC-stimulating conditions.

RESULTS

Identification of translation components that alter iRQC pathway activation

Previous studies have demonstrated that the addition of several compounds that inhibit translation initiation or activate the ISR results in uS3 and uS5 ubiquitylation.[15,17,18] Overexpression of the critical iRQC-specific E3 ubiquitin ligase RNF10, or genetic ablation of the antagonizing deubiquitylating enzyme USP10, results in degradation of the entire 40S subunit in both normal and stressed conditions.[16–18] However, other factors that contribute to iRQC activation or downstream 40S decay have not been characterized in higher eukaryotes. Because most characterized pharmacological iRQC activators inhibit translation initiation, we hypothesized that genetically perturbing translation initiation or ribosome biogenesis in a manner that impairs scanning or initiation at start codons may result in iRQC activation. To test this hypothesis, we depleted several known initiation factors and probed the extent of uS3 and uS5 ubiquitylation in the presence and absence of harringtonine (HTN), which was previously shown to stimulate uS3 and uS5 ubiquitylation. While knockdown of eIF5B, DDX3X, and DHX29 modestly decreased HTN-stimulated uS5 and uS3 ubiquitylation, eIF4A1 knockdown nearly completely inhibited ribosome ubiquitylation upon HTN treatment (Figure 1A). In stark contrast with what was observed upon eIF4A1 knockdown, knockdown of the 60S biogenesis factor eIF6 induced uS3 and uS5 ubiquitylation both with and without HTN treatment (Figures 1A and S1A). The opposing effects of eIF6 or eIF4A1 knockdown on ribosomal ubiquitylation were also observed upon treatment with the ISR activator DTT or two inhibitors that block eIF4A1 activity during scanning (Figures 1B and S1B). These results suggest that reducing eIF4A1 levels, which impairs 43S initiation complex scanning of 5′ untranslated regions (UTRs), diminishes the ribosomal population that is ubiquitylated by RNF10.

Disruption of 60S biogenesis broadly stimulates iRQC

The ribosome biogenesis factor eIF6 associates with the pre-60S ribosomal subunit during early stages of 60S biogenesis within the nucleolus and remains associated until eIF6 is released during the final cytoplasmic steps of 60S maturation.[39] To assess whether eIF6 depletion uniquely stimulates uS3 and uS5 ubiquitylation, hallmarks of iRQC activation, we depleted several characterized 60S biogenesis factors that function throughout the 60S biogenesis pathway (Figure 1C). Polysome profiling confirmed that depletion of individual 60S biogenesis factors leads to the expected reduction in free 60S subunits and 80S ribosomes without altering free 40S subunit levels (Figure 1D). Consistent with this observation, knockdown of 60S biogenesis factors resulted in a reduction in overall protein synthesis as well as reduced cell proliferation (Figures S1C and S1D). Reducing the abundance of nearly every 60S biogenesis factor tested resulted in enhanced uS3 and uS5 ubiquitylation in otherwise unperturbed cells (Figures 1E and S1E). Further analysis using mass spectrometry confirmed a significant increase in abundance of the ubiquitylated uS5-

K58 peptide upon 60S biogenesis disruption both at steady state and with HTN treatment (Figures 1F and S1F). Interestingly, depletion of EFL1 or SBDS, which act at the last step of 60S biogenesis to evict eIF6 from 60S subunits prior to 40S binding during translation initiation,[40] consistently failed to induce uS3 or uS5 ubiquitylation in multiple cell types (Figures 1E, 1F, and S1G). SBDS knockdown had no impact on overall protein synthesis or cell proliferation (Figures S1C and S1D), which suggests that SBDS plays a minor role in 60S biogenesis or overall translation activity, at least in the cell types tested here. These results indicate that disrupting 60S biogenesis at distinct steps in the pathway induces iRQC activation.

Disruption of 60S biogenesis leads to reduced 40S abundance

Reducing the abundance of translation-competent 60S subunits without impacting 40S levels results in subunit stoichiometry imbalance. Because 40S subunits engage with mRNA directly and recruit 60S subunits only at the onset of translation elongation, subunit imbalance leads to an increase in scanning preinitiation complexes that arrive at start codons and are unable to pair with 60S subunits. We hypothesized that reducing the abundance of 60S may result in a concomitant degradation of 40S subunits to partially correct the subunit imbalance. To test this hypothesis, we employed quantitative mass spectrometry to precisely measure the abundance of all ribosomal proteins in cells with and without 60S biogenesis factor depletion. The median abundance of all 60S proteins was reduced upon knockdown of five different 60S biogenesis factors, and the ratio of 60S proteins to 40S proteins was reduced upon knockdown of nearly all tested 60S biogenesis factors (Figures 2A and 2B). We confirmed the knockdown of 60S biogenesis factors using mass spectrometry and also observed that RSL24D1, eIF6, and GTPBP4 knockdown resulted in reduced levels of other 60S biogenesis factors known to act at similar steps during biogenesis (Figure S2A). Interestingly, 40S ribosomal protein abundance was also reduced upon knockdown of 60S biogenesis factors (Figure 2A). RSL24D1 and GTPBP4 knockdown resulted in a consistent reduction in all measured 60S proteins and nearly all 40S proteins (Figure 2C). This result suggests that the abundance of the entire 40S or 60S subunit is reduced upon 60S biogenesis disruption rather than a subset of ribosomal proteins. These findings are also consistent with previous observations that 60S ribosomal protein depletion in *S. cerevisiae* results in reduced 40S ribosomal protein abundance.[41]

Ribosome traffic patterns become altered upon 60S biogenesis disruption

Non-stoichiometric reduction in 60S levels relative to 40S is hypothesized to increase the amount of preinitiation complexes engaged with transcripts that fail to transition to elongating 80S ribosomes.[24] However, it is possible that unknown pathways prevent 40S engagement with mRNA when the 60S:40S ratio becomes imbalanced to prevent the accumulation of translation preinitiation complexes engaged with mRNA. Polysome profiling upon 60S biogenesis disruption demonstrated a reduction in free 60S, monosome, and polysome abundance without altering the abundance of free 40S (Figure S2B). This result suggests that 40S does not accumulate in its free form when 60S biogenesis is impaired. However, as observed previously, inhibiting 60S resulted in the formation of half-mer ribosome populations that are not observed in control knockdown cells (Figures 2D and 2E and S2B).[24–26,42,43] These half-mers migrate between canonical monosome, disome,

and trisome peaks upon sucrose gradient separation. Previous studies have hypothesized that these half-mers arise from mixtures of 40S-containing preinitiation complexes and 80S ribosomes concurrently engaged on a single transcript.[24] To more precisely define the ribosomal protein content within these half-mer populations, we separated extracts from control and GTPBP4-depleted cells on sucrose gradients and collected fractions enriched for half-mers vs. canonical monosome, disome, and trisome populations (Figures 2E and S2B). Subsequent analysis by mass spectrometry revealed that fractions comprising monosomes, disomes, or trisomes (fractions 9, 12, and 14) contained equivalent levels of 40S and 60S proteins as would be expected from 80S enriched ribosomes (Figure 2F). However, half-mer enriched fractions from GTPBP4-depleted cells displayed increased 40S:60S ratios relative to control knockdown (Figure 2F). Summing 40S and 60S protein intensity from fractions encompassing the monosome peak to the end of the gradient (fractions 9–23) revealed an increase in 40S:60S ratio upon GTPBP4 knockdown (Figure 2F). Taken together, these results suggest that lowering 60S levels relative to 40S levels results in enhanced engagement of preinitiation complexes on transcripts with elongating 80S ribosomes. Because 60S biogenesis disruption results in 40S ubiquitylation, these altered ribosome traffic patterns may contain aberrant ribosomal species that are targeted for ubiquitylation and subsequent degradation.

RNF10 is required to reduce 40S abundance upon 60S biogenesis disruption

To identify stress-responsive pathways that may be activated upon 60S biogenesis disruption, we interrogated our proteomic datasets to identify proteins whose abundance reproducibly increases upon 60S biogenesis factor knockdown. GTPBP4 knockdown results in broad changes to cellular protein levels, including the expected decrease in 60S ribosomal proteins (Figure 3A). RNF10 was among the proteins whose abundance increased upon 60S biogenesis factor knockdown (Figures 3A, 3B, and S3A–S3D). GTPBP4 knockdown resulted in increased RNF10 protein levels without significantly altering RNF10 mRNA abundance, implicating a post-transcriptional regulatory mechanism (Figure S3E). Previous studies have shown that constitutive iRQC activation leads to 40S subunit degradation in a manner that requires RNF10-dependent uS3 and uS5 ubiquitylation.[17,18] To directly examine if the reduction in 40S levels upon 60S biogenesis disruption requires RNF10 activity, we depleted GTPBP4 or RSL24D1 in our previously generated and characterized RNF10-knockout (KO) cells. Quantitative mass spectrometry analysis confirmed that both 60S and 40S proteins were reduced upon RSL24D1 and GTPBP4 knockdown (Figure 3C). While loss of RNF10 did not alter the reduction of 60S proteins upon 60S biogenesis disruption, 40S degradation was significantly attenuated upon RSL24D1 or GTPBP4 knockdown in RNF10-KO cells (Figure 3C). We confirmed that the reductions in GTPBP4 or RSL24D1 protein levels were similar in parental and RNF10-KO cells and that RNF10 abundance increased in the parental cells with 60S disruption (Figures S3F and S3G). These results demonstrate that RNF10 is required to reduce 40S abundance when 60S biogenesis is impaired.

RNF10 translation is induced upon iRQC activation in response to 60S biogenesis impairment

ISR activation results in an overall reduction in total protein synthesis while also stimulating translation of specific stress-responsive transcripts.[44] The typical mechanism governing this translation regulation involves alternative utilization of upstream open reading frames (uORFs) within the 5′ UTRs of stress-responsive transcripts.[45] To investigate possible RNF10 post-transcriptional regulatory mechanisms that are utilized to increase RNF10 protein levels upon 60S biogenesis disruption, we examined the RNF10 transcript for the presence of uORFs. The 5′ UTR of RNF10 contains three AUG start codons, which display conservation from humans to frogs (Figure S3H). Interrogating available RiboSeq datasets revealed the presence of at least four translated uORFs within the annotated RNF10 5′ UTR (Figure 3D).[46–49] We also observed a relative paucity of ribosome protected fragments within the RNF10 coding sequence (CDS) compared to the uORFs, which suggests that the uORF sequences within the RNF10 5′ UTR may repress translation of the RNF10 CDS. The two more N-terminal RiboSeq peaks within the RNF10 5′ UTR contain non-canonical initiation codons, whereas putative uORF4 and uORF5 (Figure 3D) are AUG initiated in a reading frame distinct from the RNF10 CDS start codon (Figures 3D and S3H). To test the effect of these 5′ UTR elements on RNF10 translation, we generated a translation reporter placing the RNF10 5′ UTR with the RNF10 CDS initiation sequence upstream of a dual luciferase reporter (Figure 3E). Mutation of all five putative uORF initiation codons increased *Renilla* luciferase (Rluc) expression relative to the IRES-driven firefly luciferase (Fluc) by more than 9-fold compared to the wild-type (WT) RNF10 5′ UTR, demonstrating that the uORFs repress RNF10 translation (Figure 3E). Systematic elimination of all initiation codons in isolation and all possible combinations revealed a complex regulatory structure for individual uORF sequences (Figures 3E and S3I). To test if 60S biogenesis disruption impacts RNF10 uORF-mediated translational repression, we depleted GTPBP4 and examined Rluc:Fluc expression from the WT and uORF initiation codon mutant reporters. Reducing GTPBP4 protein levels increased the Rluc:Fluc expression of the WT 5′ UTR reporter to an extent similar to the increased endogenous RNF10 protein levels (Figure 3F). Collectively, our results indicate that RNF10 translation is constitutively repressed but translationally upregulated in response to 60S biogenesis disruption by a complex and conserved uORF-dependent regulatory mechanism.

40S subunit reduction resulting from impaired 60S biogenesis requires eIF4A1

Our demonstration that HTN-induced uS3 and uS5 ubiquitylation is abrogated upon eIF4A1 knockdown indicated that active scanning of 5′ UTR sequences within transcripts may be required for 40S ubiquitylation and decay. Consistent with this hypothesis, co-knockdown of GTPBP4 and eIF4A1 prevented the reduction in 40S levels observed upon GTPBP4 knockdown alone (Figures 4A and S4A). As expected, eIF4A1 knockdown did not alter the reduction in 60S levels observed upon GTPBP4 knockdown alone (Figure 4A). Further, the increase in uS3 and uS5 ubiquitylation upon 60S biogenesis disruption was reduced with eIF4A1 knockdown as measured by immunoblotting and mass spectrometry (Figures 4B and S4B). These results suggest that mRNA engagement with the scanning preinitiation complex is required for RNF10-mediated 40S ubiquitylation when 60S abundance falls below 40S abundance.

Interestingly, RNF10 protein and mRNA abundance was decreased upon eIF4A1 knockdown in otherwise unperturbed cells (Figures 4C and S4C). Reduction of eIF4A1 also attenuated the increase in RNF10 protein levels observed upon GTPBP4 knockdown, indicating that eIF4A1-dependent scanning is required for RNF10 translational regulation (Figures 4C and S4C). Because RNF10 protein and mRNA levels are suppressed by eIF4A1 knockdown, it is possible that the observed reduction in RNF10-mediated 40S ubiquitylation and subsequent 40S degradation upon co-knockdown of eIF4A1 and GTPBP4 may be due to reduced RNF10 levels rather than reduced scanning activity. To discern between these two possibilities, we utilized 293 Flp-In cells with inducible RNF10 expression. We previously demonstrated that RNF10 overexpression alone results in reduced 40S abundance, a result that was reproduced here (Figures 4D and S4D). Knockdown of eIF4A1 reduced 40S protein decay upon RNF10 overexpression (Figures 4D and S4D), indicating that eIF4A1-dependent scanning of 5′ UTRs is required for RNF10-mediated 40S ubiquitylation and decay independent of its effect on RNF10 expression.

Ribosome splitting and canonical RQC factors are not required to reduce 40S abundance

The RNF10 ortholog in *S. cerevisiae*, Mag2, is required for the 18S NRD pathway, which degrades mutant 18S rRNA that fails to support translation elongation. This 18S NRD pathway also requires the activity of Dom34 and Slh1, which facilitate stalled 80S ribosome splitting in a manner distinct from canonical translation termination.[38] Further, a second ubiquitin ligase, Fap1, was identified as an 18S NRD factor that binds to slowly translating 80S ribosomes and extends polyubiquitin chains on Mag2 monoubiquitylated uS3.[50] We knocked down NFX1 or NFXL1, the two human proteins with the highest degree of sequence similarity to Fap1, to directly evaluate if these putative Fap1 homologs are required for 40S decay upon 60S biogenesis disruption. Unlike what was observed upon GTPBP4 knockdown in RNF10-KO cells, combined knockdown of NFX1 or NFXL1 with GTPBP4 did not reduce the 60S:40S ratio compared to GTPBP4 knockdown in isolation (Figures 5A and S5A). Further, the increase in RNF10 abundance observed upon GTPBP4 knockdown is unaffected by co-knockdown of NFX1 or NFXL1, which suggests a limited role for NFX1 or NFXL1 in the iRQC pathway (Figure S5B). To examine if known RQC pathway components function downstream of RNF10 ribosome ubiquitylation to reduce 40S abundance, we co-depleted the canonical RQC E3 ligase, ZNF598, or the ribosome splitting and rescue factors, ASCC2, ASCC3, PELO, HBS1L, and GTPBP2, with GTPBP4 and measured 60S and 40S ribosomal protein abundance by mass spectrometry. Knockdown of all tested RQC factors did not elevate 60S or 40S protein abundance relative to GTPBP4 knockdown alone (Figures 5B, S5C, and S5D). Interestingly, ZNF598, PELO, ASCC3, or GTPBP2 knockdown further reduced 40S protein levels when combined with GTPBP4 knockdown. Loss of RQC factors did not significantly alter the increased uS3 ubiquitylation observed upon GTPBP4 loss of function (Figure S5E). These observations suggest that canonical RQC factors are not required for 40S decay upon 60S biogenesis disruption and may antagonize the iRQC pathway by inhibiting 40S decay upon iRQC activation.

Reducing 40S levels attenuates iRQC activation upon 60S biogenesis disruption

Loss of 60S ribosomal proteins themselves also impairs overall 60S ribosome biogenesis and decreases 60S ribosomal abundance.[25,26,51,52] As such, we would expect to observe

a similar reduction in 40S ribosomal protein abundance upon 60S protein knockdown. Consistent with previous results in yeast,[41] uL18 (RPL5) and uL5 (RPL11) knockdown not only results in the expected decrease in 60S subunit abundance but also results in reduced 40S ribosomal protein abundance and increased RNF10 expression (Figures 5C and S5F). Interestingly, 40S ribosomal protein eS19 (RPS19) knockdown resulted in specific 40S subunit loss with no significant corresponding reduction in 60S protein levels (Figure 5C). This result suggests that RNF10-mediated 40S ubiquitylation is specifically activated when the 60S:40S ratio is reduced. We hypothesized that restoring 60S:40S stoichiometry by concomitant reduction of 40S and 60S biogenesis factors would reduce unpaired 40S levels and therefore reduce 40S ubiquitylation. Indeed, co-depletion of 40S biogenesis factors or ribosomal proteins with GTPBP4 either reduced or completely blocked uS3 and uS5 ubiquitylation compared to GTPBP4 knockdown alone (Figure 5D). This result indicates that the iRQC pathway is activated in response to an overabundance of 40S relative to 60S levels, and correcting this imbalance by depleting 40S reduces iRQC activation.

Previous studies in *S. cerevisiae* suggest that 60S binding to immature 40S intermediates in the cytoplasm assists in the final stages of 40S biogenesis.[29,30] As such, lowering 60S levels may impact late 40S biogenesis steps, resulting in the accumulation of defective 40S subunits that become incorporated into 80S ribosomes. It is possible that these improperly assembled 40S subunits represent the ribosomal species targeted by RNF10. If this is the case, then impairing the final steps of 40S maturation would stimulate RNF10-dependent 40S ubiquitylation. To test this hypothesis, we targeted the late 40S biogenesis factors NOB1, PNO1, and RIOK1, which are required for the final 18S rRNA maturation step and eS26 (RPS26) incorporation into the mature 40S subunit.[32] PNO1 but not NOB1 or RIOK1 knockdown reduced 40S protein levels (Figures S5G and S5H). Knockdown of these late 40S biogenesis factors alone failed to induce uS3 or uS5 ubiquitylation, and combining PNO1, NOB1, or RIOK1 knockdown with GTPBP4 knockdown reduced uS3 or uS5 ubiquitylation (Figures 5E and S5G). As observed for eS19, depleting eS26 reduced 40S abundance and blocked the 60S-biogenesis-disruption-mediated uS3 and uS5 ubiquitylation (Figures 5E and S5G). Further, PNO1 and eS26 knockdown reduced RNF10 protein levels in untreated and GTPBP4-depleted cells (Figure 5F). Collectively these results demonstrate that inhibiting the late steps in 40S biogenesis does not induce iRQC activation but instead impairs activation. These results are consistent with our hypothesis that RNF10 acts on scanning-competent 40S subunits rather than improperly assembled subunits.

RIOK3 is a previously uncharacterized crucial iRQC factor

To identify possible iRQC factors that act downstream of RNF10 ribosome ubiquitylation to facilitate 40S degradation, we interrogated our proteomics datasets for proteins that, like RNF10, increase in abundance upon 60S biogenesis disruption. The RIO kinase family member RIOK3 was among those proteins that reproducibly increased in abundance upon 60S biogenesis factor knockdown (Figures 6A and S6A). RIOK3 protein abundance is also elevated upon overexpression of WT, but not catalytically inactive, RNF10 (Figure S6B). Further, steady-state RIOK3 protein levels are reduced in RNF10-KO cells, and the increase in RIOK3 protein abundance observed upon knockdown of 60S biogenesis factors is significantly repressed in RNF10-KO cells (Figures S6A and S6B). The other RIO

kinase family members, RIOK1 and RIOK2, have established roles in 40S biogenesis in both yeast and mammals.[53–59] RIOK3 evolved more recently and is found only in higher eukaryotes. While RIOK3 has been demonstrated to associate with 40S subunits, RIOK3 loss-of-function does not impair 40S biogenesis.[57] In addition, an N-terminal fragment of RIOK3 was identified in a screen for ubiquitin-binding proteins.[60] These observations together led us to hypothesize that RIOK3 may act as a ubiquitin reader downstream of RNF10-mediated uS3 and uS5 ubiquitylation.

To directly test if RIOK3 contributes to 40S degradation upon iRQC pathway activation, we depleted RIOK3 alone and in combination with GTPBP4 and measured 40S abundance. Similar to RNF10 loss, RIOK3 knockdown blocked the reduction in 40S but not 60S protein levels upon GTPBP4 depletion (Figure 6B). This result was replicated in RIOK3-KO cells, indicating that RIOK3 participates in 40S decay upon 60S biogenesis disruption (Figures S6C). The increase in RNF10 protein abundance upon 60S biogenesis impairment was not inhibited by RIOK3 loss of function (Figures 6D and S6D). Interestingly, uS3 and uS5 ubiquitylation was substantially increased by combining RIOK3 and GTPBP4 knockdown compared to GTPBP4 knockdown alone (Figure 6C). This suggests that loss of RIOK3 leads to elevated levels of ubiquitylated 40S ribosomes that cannot be degraded. These results demonstrate that ribosome ubiquitylation alone is not sufficient to facilitate 40S degradation and that RIOK3 acts downstream of RNF10-mediated ribosome ubiquitylation to facilitate 40S decay.

RIOK3 ubiquitin binding is necessary for 40S decay

Examination of the RIOK3 amino acid sequence, sequence conservation, and predicted AlphaFold structure reveals three general domains: a predicted ubiquitin-binding N-terminal domain, a conserved helical linker domain, and a RIO kinase domain (Figures 7A and S7A). The putative N-terminal ubiquitin-binding domain contains two inverted ubiquitin interaction motifs (MIU1/2).[61–63] AlphaFold3 modeling of the RIOK3 N-terminal domain with ubiquitin highlighted a binding surface comprising hydrophobic MIU residues known to interact with ubiquitin and the well-characterized hydrophobic patch on ubiquitin centered on I44 (Figures 7A and S7B–S7D). Consistent with structural modeling and previous data, WT RIOK3, but not a mutant version of RIOK3 that lacks the ubiquitin-binding domains (Δ1–153; ΔN hereafter), associated with polyubiquitin as demonstrated by co-immunoprecipitation experiments (Figures 7B and 7C). Mutation of two catalytic residues within the kinase domain (K290A/D406A, KM hereafter) did not impair ubiquitin binding (Figures 7B and 7C).

To test if RIOK3 ubiquitin binding or kinase activity was necessary for RIOK3 to facilitate 40S decay, we performed knockdown rescue experiments using RIOK3 transgenes that are resistant to small interfering RNAs (siRNAs) used to deplete endogenous RIOK3. Consistent with previous results, RIOK3 knockdown prevented the reduction in 40S protein levels observed upon GTPBP4 depletion. The reduction in 40S protein levels was restored upon expression of WT but not ΔN or KM RIOK3, indicating that both kinase activity and ubiquitin binding are necessary for RIOK3 to facilitate 40S decay (Figures 7D and S7G). Similarly, expression of WT but not ubiquitin-binding-deficient RIOK3 reduced

uS3 and uS5 ubiquitylation observed upon GTPBP4 knockdown (Figure 7E). Interestingly, expression of the kinase mutant RIOK3 resulted in elevated uS3 and uS5 ubiquitylation, suggesting that kinase-inactive RIOK3 may block deubiquitylating enzyme access to ubiquitylated 40S (Figure 7E). The results establish that RIOK3 ubiquitin binding and kinase activities are required to facilitate 40S decay.

Depleting amino acids induces 40S decay

Our results, combined with results from others,[41,51,64] demonstrate that lowering 60S protein abundance results in 40S ubiquitylation and degradation. We previously demonstrated that uS3 and uS5 ubiquitylation is stimulated upon conditions that activate the ISR, which suggests that chronic ISR activation may also result in iRQC-dependent 40S decay.[15,17] To investigate this hypothesis, we cultured cells in medium without lysine and arginine, as this amino acid starvation paradigm is known to induce the ISR via ribosome p-stalk-mediated GCN2 activation.[65] We measured ribosomal protein abundance via mass spectrometry in cells grown in lysine/arginine-free medium over a 96-h time course. Imbalanced ribosome subunit stoichiometry due to reduced 40S relative to 60S (high 60S:40S ratio) was observed after 24 h of amino acid starvation (Figure 7F). This stoichiometry imbalance worsened after 24 h, with a more than 20% increase in 60S relative to 40S observed after 96 h of lysine and arginine depletion. The subunit stoichiometry imbalance observed upon amino acid starvation was blocked in either RNF10- or RIOK3-KO cells, indicating that 40S decay in this context is also mediated by iRQC factors (Figures 7F, S7E, and S7F). Despite the large difference in ribosome stoichiometry, the ISR is similarly activated in RNF10-KO and RIOK3-KO cells as judged by ATF4 protein expression (Figure S7H). Indicative of iRQC activation, RIOK3 levels increased over time when culturing cells in lysine/arginine-free medium (Figure S7I). These results establish that chronic ISR stimulation results in iRQC activation and subsequent RIOK3-dependent 40S decay. Collectively, our findings establish that diverse conditions that impair translation initiation result in RNF10-mediated 40S ubiquitylation, and RIOK3 acts as a ubiquitin receptor for these 40S subunits to facilitate their degradation (Figure 7G).

DISCUSSION

Biologically relevant contexts for iRQC pathway activation

A variety of defects within ribosomes or mRNA can impair ribosome progression that, left unresolved, would reduce the pool of available ribosomes and lower cellular protein biogenesis capacity.[2–4] Ribosome ubiquitylation has emerged as a key step in regulating ribosome-associated quality control (RQC) pathways.[66] A growing number of ubiquitin ligases facilitate site-specific ubiquitylation of individual ribosomal proteins in response to distinct perturbations that impede ribosome progression.[15,17,67,68] While ISR agonists, translation initiation inhibitors, and high-dose translation elongation inhibitors all induce RNF10-dependent uS3 and uS5 ubiquitylation, how this pathway is activated in the absence of chemical agonists was unclear. USP10 depletion results in chronic uS3 and uS5 ubiquitylation and reduced 40S abundance in the absence of stress, which suggests that RNF10-dependent ubiquitylation may occur as part of the normal translation cycle.[16,17] We demonstrate that either direct disruption of the 60S:40S stoichiometry by limiting 60S

biogenesis activity or chronic ISR induction by limiting amino acid availability elevates uS3 and uS5 ubiquitylation and stimulates 40S decay. These findings illuminate biologically relevant cellular stress conditions that utilize this surprising 40S decay pathway to abrogate translational stress.

Mutations in a variety of genes encoding ribosomal proteins result in a diverse collection of human ribosomopathies.[69] Diamond-Blackfan anemia (DBA) is among these ribosomopathies where heterozygous loss-of-function mutations in many different ribosomal protein genes result in impaired erythropoiesis.[70] Studies examining the effect of DBA-associated ribosomal protein loss in human cells revealed that reducing 60S proteins results in loss of both large and small subunit ribosomal proteins, whereas depleting 40S ribosomal proteins had a minor effect on 60S ribosomal protein abundance.[51] These observations mirror our results, suggesting that RNF10-dependent 40S decay occurs in a subset of DBA patients with mutations that selectively compromise 60S ribosome assembly. These observations are consistent with studies in yeast showing that the expression of non-functional 60S ribosomal protein mutants results in a general loss in both ribosomal subunits, whereas expression of 40S mutants has no corresponding effect on 60S abundance.[41] Proteasomal gene expression is also induced solely with the expression of 60S mutants in these yeast studies. These data suggest the presence of conserved cellular mechanisms that specifically target excess 40S ribosomal proteins for degradation when 40S abundance exceeds 60S.

Acute ISR pathway activation stimulates RNF10-dependent uS3 and uS5 ubiquitylation in a manner that requires eIF2α phosphorylation.[15] Here, we show that chronic ISR activation via amino acid starvation also results in 60S:40S imbalance through selective 40S decay (Figure 7F). Similar to what we observe when 60S biogenesis is blunted, this 40S decay pathway also requires RNF10 and RIOK3. We also observe a general decrease in both 40S and 60S abundance in RNF10- or RIOK3-KO cells, indicative of a global increase in ribosome flux through the autophagy pathway that is activated upon amino acid starvation (Figures S7E and S7F).[71] The iRQC-dependent 40S decay appears to operate separate from this general autophagic ribosomal degradation pathway to further limit 40S abundance when protein biosynthesis building blocks become limiting. It remains unclear whether this conserved 40S decay pathway provides a selective advantage during starvation conditions. Because several distinct initiation stress conditions that lead to diverse ribosomal outcomes all lead to iRQC activation, it remains unclear what precise ribosomal species RNF10 recognizes for ubiquitylation. Structural studies under various initiation inhibition conditions will be necessary to determine how RNF10 recognizes 40S subunits in these distinct contexts (Figure 7G).

Similarities and distinctions between mammalian iRQC and yeast NRD pathways

The mammalian iRQC pathway bears some similarities to the established 18S NRD pathway in yeast. Mutations in 18S rRNA lead to uS3 ubiquitylation by the RNF10 ortholog, Mag2, at the same conserved residue of yeast uS3 that RNF10 utilizes for mammalian 40S decay.[38] While the initial ubiquitylation event and ubiquitin ligase are conserved, there are notable differences between the mammalian iRQC and the yeast 18S NRD pathways. First,

knockdown of the proposed human homologs of Fap1, NFX1, and NFX1L fails to rescue the reduction in 40S levels observed upon 60S biogenesis disruption. Furthermore, the resolution of the 18S NRD pathway requires the ribosome disassociation factors Dom34 and Slh1, both of which play integral roles in the canonical RQC pathway. Knockdown of Pelota or ASCC3, the Dom34 and Slh1 homologs, did not impair iRQC-mediated 40S decay, indicating that stalled ribosome disassociation is not required to reduce 40S levels when 60S biogenesis is inhibited. This finding is consistent with *in vitro* studies demonstrating that the ASCC2/3 complex did not appreciably dissociate 80S ribosomes that were ubiquitylated by RNF10.[72] Further, the yeast genome does not contain a clear RIOK3 ortholog. These observations collectively suggest that, despite similarities in the initiating ubiquitylation event, the downstream mechanisms leading to 40S degradation may have diverged during evolution.

It remains possible that other, NRD-like, pathways exist to target defective or improperly assembled 40S ribosomes for degradation. In support of this idea, previous studies identified the deubiquitylating enzyme USP16 as a late-acting 40S biogenesis factor. Depleting USP16 increased 40S ubiquitylation on a specific lysine residue of eS31 but failed to alter uS3 or uS5 ubiquitylation, implicating other ubiquitylation enzymes in the targeting of improperly assembled 40S.[73] Consistent with these findings, we show that loss of late 40S biogenesis factors does not induce iRQC activation and instead reduces uS3 and uS5 ubiquitylation upon 60S biogenesis loss. Further, recent studies documenting a role for the yeast Rio1 kinase in a 40S assembly quality control pathway show that this pathway co-opts Hel2, but not Mag2-dependent ribosome ubiquitylation.[74]

A feedforward mechanism of iRQC activation and 40S decay

Our results demonstrate that iRQC capacity is generally regulated under iRQC-activating conditions by increasing the abundance of both RNF10 and RIOK3. RNF10 protein levels are regulated by a translation control mechanism that utilizes conserved uORFs within the 5′ UTR of the RNF10 transcript. Our reporter results indicate that RNF10 uORFs suppress RNF10 translation under normal cellular conditions. However, upon disrupting 60S biogenesis, translation from the RNF10 start codon is increased. This leads to an interesting model where conditions that favor stalled preinitiation complexes, the putative triggering event for iRQC, also inherently favor increased RNF10 expression. RIOK3 protein levels also increase upon conditions that stimulate iRQC pathway activation, including amino acid starvation (Figure S7I). Our findings suggest that RIOK3 binds ubiquitylated 40S ribosomes downstream of RNF10 activity, which positions RIOK3 as a crucial reader that helps interpret the ribosome ubiquitin code. RIOK3 uses tandem MIUs to bind ubiquitin. MIU domains from Rabex-5 and MINDY-1 have been shown to interact with ubiquitin using the canonical hydrophobic patch of ubiquitin.[61–63] AlphaFold structural modeling also predicts that the MIU domains of RIOK3 interact with ubiquitin using similar interaction surfaces (Figure 7A). The tandem MIU domains found in the MINDY-1 deubiquitylating enzyme show a binding preference for K48-linked polyubiquitin, and structural studies reveal that a single MINDY-1 MIU domain can interact with three separate ubiquitin entities with the polyubiquitin chain using distinct MIU binding sites.[63] Similarly, AlphaFold structural modeling predicts interaction of the RIOK3 tandem MIUs with multiple ubiquitin

molecules (Figure S7B). These observations raise the intriguing possibility that the tandem MIU domains within RIOK3 may be used to engage 40S with multiple ubiquitin moieties that occur from concurrent uS3 and uS5 ubiquitylation events. This mode of ubiquitin engagement may provide the mechanistic rationale for why both uS3 and uS5 ubiquitylation events are required for iRQC-mediated 40S decay.

Limitations of the study

Using quantitative mass spectrometry to measure ribosome abundance, we document a 10%–20% decrease in 40S abundance upon iRQC pathway activation. The source of the variability when measuring 40S abundance could arise from a variety of both known and unknown factors. We do not know the extent of pathway activation in other cell or tissue types or how varying cellular conditions may modify iRQC pathway activity. For example, a 10-fold overexpression of RNF10 results in a 13% decrease in 40S abundance. These results suggest there are other limiting factors, like the specific 40S conformation that allows for RNF10-dependent ubiquitylation, that contribute to 40S decay. This study does not define the ribosomal species targeted by RNF10 and RIOK3. While our results suggest that the iRQC pathway acts on 40S subunits during scanning or initiation, RNF10 may recognize any number of related molecular species, including slowly translating 80S ribosomes or unique collision interfaces. Similarly, it is unclear how chronic ISR induction, which limits 43S recruitment to mRNA, results in iRQC pathway activation. Structural and biochemical studies will be necessary to determine the precise ribosomal species that recruits RNF10. We combine sucrose gradient density centrifugation and proteomic analysis to characterize half-mer-enriched fractions. While sucrose density centrifugation is routinely used to examine distinct ribosomal populations, separation by density alone cannot conclusively identify the molecular constituents of ribosomal populations within individual fractions.

RESOURCE AVAILABILITY

Lead contact

Requests for further information and resources and reagents should be directed to and will be fulfilled by the lead contact, Eric Bennett (e1bennett@ucsd.edu).

Materials availability

All reagents generated in the study are available from the lead contact with a completed materials transfer agreement.

Data and code availability

- All raw mass spectrometry proteomics data have been deposited with the ProteomeXchange Consortium via the PRIDE partner repository with the dataset identifiers listed in the key resources table.
- This paper does not report original code.
- Any additional information required to reanalyze the data reported in this paper is available from the lead contact upon request.

STAR★METHODS

Detailed methods are provided in the online version of this paper and include the following:

EXPERIMENTAL MODEL AND STUDY PARTICIPANT DETAILS

Cell lines and culture conditions—HEK293T (female) and 293Flp-In (female) cells were grown in DMEM (ThermoFisher: 11995065) supplemented with 10% fetal bovine serum (FBS) and 1% penicillin/streptomycin and maintained at 37°C in a 5% CO2 humidified incubator. HAP1 (male derived, lacking a Y chromosome) cells were grown in IMDM (ThermoFisher: 12440053) supplemented with 10% fetal bovine serum (FBS) and 1% penicillin/streptomycin and maintained as above. OVTOKO (female) cells were grown in RPMI (Fischer Scientific: SH30027FS) supplemented with 10% fetal bovine serum (FBS) and 1% penicillin/streptomycin and maintained as above. These commercial cell lines were not reauthenticated during the course of this study. Cell cultures were tested for mycoplasma contamination monthly.

METHOD DETAILS

siRNA knockdown—All siRNA knockdown experiments were performed by reverse transfection using Lipofectamine RNAiMAX (Thermo Fisher) according to manufacturer instructions. siRNA from a 10uM stock was plated in OptiMEM medium (Thermo Fisher) to a concentration of 500nM, RNAiMAX was added at a 2:1 ratio to the siRNA by volume and incubated for 20 minutes. Cells were counted and diluted to a concentration of 3×10^5/mL then added to the transfection mix at a ratio of 4:1 cell suspension to OptiMEM by volume. Cells were expanded at 24hrs post transfection to avoid over confluence. All knockdown cells were harvested at 72hrs post transfection. For HTN experiments, cells were treated prior to harvesting cells with 2ug/ml HTN for 2 hours. A list of all RNAi oligonucleotides used in this study can be found in Table S1.

Immunoblotting—For all immunoblot analysis, cell pellets were resuspended in urea denaturing lysis buffer (8M urea, 50mM Tris-Cl, pH 8.0, 75mM NaCl, 1mM NaV, 1mM NaF, 1mM β-glycerophosphate, 40mM NEM in the presence of EDTA-free protease inhibitor cocktail) and kept on ice during preparation. Cell lysates were sonicated for 10s (output of 3W on a membrane dismembrator model 100, Fisher Scientific) with a microtip probe then centrifuged for 10 min at 15,000rpm at 4°C. Lysate protein concentrations were measured by BCA Protein Assay (23225, Thermo Scientific Pierce). Laemmli sample buffer with β-mercaptoethanol was then added to cell lysates and heated at 95°C for 5 min. Samples were then cooled to room temperature and centrifuged briefly. Lysates were resolved on 12% Tris-glycine SDS-PAGE gels, followed by transfer to PVDF membranes (1620177, BioRad) using Bjerrum semi-dry transfer buffer (48mM Tris Base, 39mM Glycine-free acid, 0.0375% SDS, 20% MeOH, pH 9.2) and a semi-dry transfer apparatus (Bio-Rad Turbo Transfer) for 30 min at 25V. Immunoblots were blocked with 5% blotting grade nonfat dry milk (APEX Bioresearch) in TBST for 1 hour. Primary antibodies were diluted in 5% BSA and rocked overnight. Immunoblots were developed using Clarity Western ECL Substrate (1705061, BioRad) and imaged on a Bio-Rad Chemi-Doc XRS+

system. All blots were processed Bio-Rad Image Lab software (RRID:SCR_014210), with final images prepared in Adobe Illustrator.

Puromycin protein synthesis assay—For the protein synthesis assay, 293T cells were transfected with the indicated siRNA as described above. Cells were treated with 2uM puromycin or 100ug/mL CHX for 30 minutes prior to harvesting. Cell pellets were lysed and immunoblotted for puromycin incorporation as described above. Extent of puromycin incorporation was quantified by calculating the overall intensity of each lane using Bio-Rad Image Lab software (RRID:SCR_014210).

Proliferation assay—For the proliferation assay, siRNA transfections were performed in sterile 1.5mL tubes at the concentrations indicated previously. In brief, 1uL of a 10uM stock solution of each siRNA oligo and 2uL of Lipofectamine RNAiMAX were added to 200uL OptiMEM medium (Thermo Fisher) in sterile 1.5mL tubes. 293T cells were counted and diluted to a concentration of 6.25×10^4/mL then 800uL of the cell suspension was added to each transfection mix. Each mix was aliquoted into 5 non-edge wells of a white opaque 96-well plate (3917, Corning), 100uL each aliquot, equating to 5000 cells plated per well. Empty media was added to the remaining wells. Cells were incubated and allowed to grow for 72 hours. At 72 hours post transfection, the CellTiter-Glo assay was carried out according to the manufacturer's instructions (G9243, Promega). The assay plate was equilibrated to room temperature for 30 minutes, 100uL of CellTiter-Glo reagent was added to each well, and the plate was shaken on an orbital shaker for 2 minutes. The assay plate was left at room temperature without shaking for 10 minutes to stabilize luminescent signal. Luminescence was then read using a Promega GloMax-96 well microplate reader (9100–100, Turner Biosystems, Promega) running the CTG protocol in the GloMax®-96 Software (Promega). Each condition was normalized to siControl luminescence.

Mass spectrometry sample preparation and analysis—For all mass spectrometry analysis, cell pellets were resuspended in urea denaturing lysis buffer without protease inhibitors (8M urea, 50mM Tris-Cl, pH 8.0, 75mM NaCl, 1mM NaV, 1mM NaF, 1mM β-glycerophosphate, 100mM IAA) and kept on ice during preparation. Cell lysates were sonicated for 10s (output of 3W on a membrane dismembrator model 100, Fisher Scientific) with a microtip probe then centrifuged for 10 min at 15,000rpm at 4°C. Lysate protein concentrations were measured by BCA Protein Assay (23225, Thermo Scientific Pierce). 20ug of protein for each sample was diluted in 140uL of 50mM Tris-Cl. Samples were reduced with 10mM TCEP for 30min, then alkylated with 15mM IAA for 45min in the dark. Excess IAA was inactivated with 10mM DTT for 15 minutes. Samples were then diluted with 200uL of 50mM Tris-Cl to ensure urea concentration below 1M and a pH of at least 7 for efficient digestion. pH was validated using universal tester strips and an additional 50mM Tris-Cl was added as needed. 200ng of Lys-C (121–05063, FUJIFILM Wako Pure Chemical Corporation) and 500ng mass spectrometry grade Trypsin (V511, Promega) were added, and samples were incubated while shaking at 37°C overnight. For peptide cleanup, stage tips were prepared using C18 membranes (Empore, Sigma, 66883-U). Cleaned and dried peptides were resuspended in 20uL 5% acetonitrile/5% formic acid, centrifuged at maximum speed for 1 minute, then 18uL of the solution was moved to

an autosampler vial (Waters, 186009186) with a preslit silicone cap (Waters, 186005827). Samples were analyzed on the timsTOF Pro 2 mass spectrometer platform (Bruker) coupled with a nanoElute 2 for HPLC (Bruker) using a 25cm × 150um PepSep column (Bruker, C18 resin, 1.5 angstrom pore size). 1uL (equivalent to 1ug of starting protein) of each sample was injected onto the column and peptide separation was carried out using a 50 minute linear 5%–35% acetonitrile gradient. Data was acquired in data independent analysis Parallel Accumulation Serial Fragmentation (diaPASEF) with an MS1 range of 100–1700 m/z. The isolation windows were designed to encompass the precursor distribution across the m/z-1/k0 plane as defined by previous ddaPASEF data, ranging from 323.6 to 1221.6 m/z and 0.7 to 1.34 V s/cm2 in 1/k0. Each 75 ms diaPASEF scan spanned a 40 Da mass width with a 1 Da mass overlap, with 50 windows and 25 PASEF cycles to cover the entire ion mobility spectrum. This isolation window scheme was designed using the publicly available python package py_diAID[75]. Data was searched with an *in silico* generated library using DIA-NN software[76] with the following settings. Library generation: Trypsin/P protease, 2 missed cleavages allowed, 2 variable modifications allowed, N-term M excision allowed, C carbamidomethylation selected, M oxidation, N-term acetylation, peptide length range 7–30, precursor charge range 2–4, precursor m/z range 300–1800, fragment ion m/z range 200–1800. Search settings: use isotopologues selected, MBR selected, no shared spectra selected, mass accuracy 10.0, MS1 accuracy 10.0, protein interference – genes, neural network classifier – single-pass mode, quantification strategy – robust LC, cross-run normalization – RT-dependent, speed and RAM usage – optimal results. Data were also searched using the same settings for diglycine remnant-containing peptide library provided by the Eric Fischer (Dana-Farber Cancer Institute). The mass spectrometry proteomics data have been deposited to the ProteomeXchange Consortium via the PRIDE partner repository with the dataset identifiers listed in the Key Resources Table.

Sucrose density gradient fractionation—Cells were briefly washed in ice cold PBS with 150ug/mL cycloheximide (CHX) before harvesting. Cell pellets were lysed in 700uL of lysis buffer (20mM Tris-Cl, pH 8.0, 150mM NaCl, 15mM MgCl2, 1% Triton-X 100, 40U Turbo DNase I, 40mM NEM, 1mM DTT, EDTA-free protease inhibitor cocktail in DEPC treated water) followed by vigorous pipetting and incubated on ice for 15min. The cell lysates were centrifuged at 15,000 rpm for 10min at 4°C and the supernatant was transferred to a new microcentrifuge tube. Total RNA concentration of each lysate was determined using a nanodrop (Thermo Scientific). 300ug of total RNA for each sample was fractionated over a 10–50% sucrose gradient containing 150ug/mL CHX, 1mM DTT, and 2U/mL SUPERase-In (prepared on Gradient Master 108, Biocomp: 1min 54s, 81.5 degrees, 16rpm). Samples were centrifuged at 41,000rpm for 2hrs at 4°C in an SW41i rotor. 1ml fractions were collected using a PGFip piston gradient fractionator (Biocomp). Protein fractions were precipitated overnight with 10% TCA at 4°C, followed by three ice-cold acetone washes. Pellets were dried in Vacufuge plus (Eppendorf) at room temperature for 5 min. Protein pellets were resuspended in 50uL 8M Urea, 50mM Tris-Cl and processed for mass spectrometry as described above, skipping the lysis and quantification steps and substituting 10mM NEM (instead of IAA) for alkylation.

RNF10 qPCR analysis—For qPCR analysis, cells were subjected to siRNA knockdown as described above. 72 hours post transfection cells were collected in TRIzol and 1/5th volume of chloroform was added. Samples were centrifuged at 12,000g for 15 minutes at 4°C and the aqueous layer was transferred to a new tube. RNA was precipitated using 500uL isopropanol, centrifuged at 12,000g for 10 minutes at 4°C, resuspended in 1mL 75% ethanol, centrifuged at 7,500g for 5 minutes at 4°C, then vacuum dried for 5 minutes. RNA was resuspended in 50uL DEPC-treated water and incubated at 55°C for 10 minutes. cDNA was synthesized using the SuperScript III First Strand Synthesis system (18080–051, Invitrogen). 4ul of each sample was plated into a 96-well thermocycler plate, followed by 4uL of nuclease free water, and 12ul of master mix containing iTaq Universal SYBR Green Supermix (1725121, BioRad) and primers for gene of interest. The following PCR conditions were run on a C1000 Thermo Cycler (BioRad): 50°C for 10min, 95°C for 15min, 95°C for 10s, 60°C for 30s (repeat for 40 cycles). All relative quantifications were calculated using the delta delta Ct method relative to the housekeeping gene GAPDH, equivalent to $\log_2$ fold change. A list of qPCR primers used in this study can be found in the Table S1.

RNF10 overexpression—The RNF10 overexpression experiment was performed using our previously generated 293FlpIn-FRT-Flag-HA-RNF10wt inducible cell line[17]. Knockdown of eIF4A1 in these cell lines was performed as described above. After 24 hours, expression of RNF10 was induced with doxycycline treatment at 2ug/mL. Cells were collected at 72 hours post-knockdown and processed for proteomics as described above.

Reporter construct cloning and reporter assay—The RNF10 5’UTR was amplified from the cDNA generated from the prior qPCR experiment and inserted into pcDNA3-RLUC-IRES-FLUC (Addgene, #45642). Mutations were introduced using QuickChange site-directed mutagenesis utilizing PCR-based approaches. Template DNA was digested by Dpn1 followed by transformation of the mutated plasmids into TOP10 E. coli cells. Plasmids were confirmed by sequencing. A list of primers used in this study can be found in the Table S1. The reporter assay was performed by preparing transfection mixes for all reporter constructs using Lipofectamine 2000 (11668027, Thermo Fisher). 300ng of reporter construct plasmid was added to 30uL of OptiMEM medium (Thermo Fisher). 1.05uL Lipofectamine 2000 was added to each transfection mix. 10uL of the transfection mix was aliquoted into 3 wells of a white opaque 96-well plate (3917, Corning) for each reporter. 10000 293 Flp-In cells were plated in each well. 24 hours post-transfection media was aspirated out of the plate and replaced with 80uL PBS. Firefly and renilla luciferase activity were quantified using the Promega dual-glo luciferase assay system (Promega, E2940). 80uL of Dual-Glo reagent was added to each well, and the plate was shaken on an orbital shaker for 15 minutes. Firefly luminescence was read out using a Promega GloMax-96 well microplate reader (9100–100, Turner Biosystems, Promega) running the Dual-glo protocol in the GloMax®-96 Software (Promega). 80uL of Stop & Glo reagent was added to each well, and the plate was shaken on an oribital shaker for 15 minutes. Renilla luminescence was read out using a Promega GloMax-96 well microplate reader (9100–100, Turner Biosystems, Promega) running the Dual-glo protocol in the GloMax®-96 Software (Promega). Rluc:Fluc ratios were quantified and normalized to the WT 5’UTR reporter. For the subsequent reporter assay with GTPBP4 loss, cells were first plated in

6-well dishes in order to give ~70% confluence the following day. Cells were transfected with reporter constructs using Lipofectamine 3000 (L3000001, Thermo Fisher) according to the manufacturer protocol using 250uL OptiMem medium, 2500ng reporter construct DNA, 5uL P3000 reagent, and 7.5uL Lipofectamine 3000. 24-hours post-transfection, cells were counted and diluted for reverse transfection with siControl and siGTPBP4 as described previously at a 24-well scale. At 72 hours post-knockdown, the cells in each well were collected, resuspended in 80uL 1X PBS, and moved to individual wells of a white opaque 96-well plate (3917, Corning). Luciferase activity was measured using the Promega dual-glo luciferase assay system (Promega, E2940) as described above.

RIOK3 mutant construct cloning and rescue experiment—The RIOK3 CDS in pDONR233 was obtained from the hORFeome V8.1 library (BROAD Institute[77]). Mutations were introduced using QuickChange site-directed mutagenesis utilizing PCR-based approaches. Template DNA was digested by Dpn1 followed by transformation of the mutated plasmids into TOP10 E. coli cells. Plasmids were confirmed by sequencing. A list of primers used in this study can be found in the Table S1. The RIOK3 mutants were then cloned into a pHAGE-NTAP-IRES-PURO destination vector using Gateway cloning (Invitrogen). Using Mirus TransIT 293 transfection reagent, 293Flp-In cells were transfected with five helper plasmids pHAGE-GAG-POL; pHAGE-VSVG; pHAGE-tat1b; pHAGE-rev and the RIOK3 WT and mutant constructs (wild type or catalytic mutant), followed by the addition of fresh media after 24 hours. The supernatant was filtered using a 0.45 mm sterile syringe filter and mixed with 2ul of 6mg/ml polybrene. The viral mixture was then added to cells seeded at 50% confluency and infected for 24hours. Stable expression clones were selected with 1ug/ml Puromycin. Expression of the constructs was validated by immunoblotting for RIOK3 and FLAG. Rescue experiment was performed in triplicate using the siRNA oligo that the RIOK3 constructs were hardened against (oligo #1). Knockdown, immunoblotting, and proteomic analyses were performed as described above.

RIOK3 KO cell line generation—RIOK3 knockout was done using CRISPR/Cas9 genome engineering in 293Flp-In cells. A single validated guide RNA sequence for human cells (Horizon Discovery, 5'-ACCGGTTCCCACTCCTAAAA-3') was cloned into a pSpCas9(BB)-2a-GFP plasmid (Addgene, #48138). Cells were transfected with the plasmid containing the guide RNA using lipofectamine 2000. 48 hours post transfection, GFP positive cells were sorted on a BD FACSAria Fusion (BD BioSciences) cell sorter. Pooled cell sorts were clonally isolated by limiting dilution method. Clonal lines were validated for loss of RIOK3 by immunoblotting and mass spectrometry.

RIOK3 immunoprecipitation assay—Cells expressing the indicated RIOK3 transgene were lysed by incubating on ice in 50 mM Tris pH 8.0, 150 mM NaCl, 0.5% NP-40, 1 mM β-glycerophosphate, 1 mM NaF, 1 mM sodium orthovanadate, 100 mM IAA in the presence of EDTA-free protease inhibitor cocktail Lysates were cleared by centrifugation at 15,000 rpm for 10 min at 4°C. Protein concentrations were determined by BCA Protein assay (Thermo Fisher). 150ug of protein from each sample was incubated with 30uL anti-HA agarose beads for 2 h at 4°C. The beads were washed three times with 50 mM Tris pH 8.0, 150 mM NaCl, 0.1% NP-40. After complete removal of wash buffer, beads were boiled

in 50uL 2X Laemmli sample buffer and boiled to elute protein. Immunoblotting was then carried out using the indicated antibodies as described above.

Amino acid starvation assay—Parental 293Flp-In cells, RNF10KO cells, and RIOK3 KO cells were plated overnight in standard DMEM (ThermoFisher: 11995065) in 6-well dishes to give a confluence of ~40% for the assay. Adhered cells were gently washed with PBS before media replacement using DMEM for SILAC lacking arginine and lysine (ThermoFisher: 88364) supplemented with dialyzed FBS. Amino acid deprived cells were collected at the indicated timepoints and processed for proteomic analysis as described above.

QUANTIFICATION AND STATISTICAL ANALYSIS

All mass spectrometry experiments were performed in triplicate (n=3) as biologically distinct samples unless otherwise indicated in the figure legends. Median ribosomal protein abundance was determined by mass fraction normalization. All comparisons were done to the relevant control or siGTPBP4 conditions as indicated in the figure legends. Significance (p-value) was determined using unpaired two-tailed Student's t-test in Microsoft Excel. Volcano plots were generated using limma analyses[78] from maxLFQ normalized data output from DIA-NN. Significance between conditions in the amino acid starvation experiments was determined with two-way analysis of variance (ANOVA) followed by the appropriate multiple comparisons test (Tukey's HSD or Dunnett's) as indicated in the figure legends using GraphPad Prism 10.2.3.

Supplementary Material

Refer to Web version on PubMed Central for supplementary material.

ACKNOWLEDGMENTS

We thank Katherine Donovan and Eric Fischer (Dana Farber Cancer Institute) for providing the diGLY-modified peptide library for data analysis. Figure 1C was created with Biorender.com. Research funding was provided by an NIH Training Program to P.W.F. and D.M.G. (T32GM133351) and NIH research support to E.J.B. (R35GM148339 and R01GM136994).

REFERENCES

1. Pelletier J, and Sonenberg N (2019). The Organizing Principles of Eukaryotic Ribosome Recruitment. Annu. Rev. Biochem. 88, 307–335. 10.1146/annurev-biochem-013118-111042. [PubMed: 31220979]
2. D'Orazio KN, and Green R (2021). Ribosome states signal RNA quality control. Mol. Cell 81, 1372–1383. 10.1016/j.molcel.2021.02.022. [PubMed: 33713598]
3. Yip MCJ, and Shao S (2021). Detecting and Rescuing Stalled Ribosomes. Trends Biochem. Sci. 46, 731–743. 10.1016/j.tibs.2021.03.008. [PubMed: 33966939]
4. Filbeck S, Cerullo F, Pfeffer S, and Joazeiro CAP (2022). Ribosome-associated quality-control mechanisms from bacteria to humans. Mol. Cell 82, 1451–1466. 10.1016/j.molcel.2022.03.038. [PubMed: 35452614]
5. Meydan S, and Guydosh NR (2021). A cellular handbook for collided ribosomes: surveillance pathways and collision types. Curr. Genet. 67, 19–26. 10.1007/s00294-020-01111-w. [PubMed: 33044589]

6. Vind AC, Genzor AV, and Bekker-Jensen S (2020). Ribosomal stress-surveillance: three pathways is a magic number. Nucleic Acids Res. 48, 10648–10661. 10.1093/nar/gkaa757. [PubMed: 32941609]
7. Brandman O, Stewart-Ornstein J, Wong D, Larson A, Williams CC, Li GW, Zhou S, King D, Shen PS, Weibezahn J, et al. (2012). A ribosome-bound quality control complex triggers degradation of nascent peptides and signals translation stress. Cell 151, 1042–1054. 10.1016/j.cell.2012.10.044. [PubMed: 23178123]
8. Ikeuchi K, Tesina P, Matsuo Y, Sugiyama T, Cheng J, Saeki Y, Tanaka K, Becker T, Beckmann R, and Inada T (2019). Collided ribosomes form a unique structural interface to induce Hel2-driven quality control pathways. EMBO J. 38, e100276. 10.15252/embj.2018100276. [PubMed: 30609991]
9. Juszkiewicz S, Chandrasekaran V, Lin Z, Kraatz S, Ramakrishnan V, and Hegde RS (2018). ZNF598 Is a Quality Control Sensor of Collided Ribosomes. Mol. Cell 72, 469–481. 10.1016/j.molcel.2018.08.037. [PubMed: 30293783]
10. Simms CL, Yan LL, and Zaher HS (2017). Ribosome Collision Is Critical for Quality Control during No-Go Decay. Mol. Cell 68, 361–373. 10.1016/j.molcel.2017.08.019. [PubMed: 28943311]
11. Sundaramoorthy E, Leonard M, Mak R, Liao J, Fulzele A, and Bennett EJ (2017). ZNF598 and RACK1 Regulate Mammalian Ribosome-Associated Quality Control Function by Mediating Regulatory 40S Ribosomal Ubiquitylation. Mol. Cell 65, 751–760. 10.1016/j.molcel.2016.12.026. [PubMed: 28132843]
12. Juszkiewicz S, and Hegde RS (2017). Initiation of Quality Control during Poly(A) Translation Requires Site-Specific Ribosome Ubiquitination. Mol. Cell 65, 743–750. 10.1016/j.molcel.2016.11.039. [PubMed: 28065601]
13. Matsuo Y, Tesina P, Nakajima S, Mizuno M, Endo A, Buschauer R, Cheng J, Shounai O, Ikeuchi K, Saeki Y, et al. (2020). RQT complex dissociates ribosomes collided on endogenous RQC substrate SDD1. Nat. Struct. Mol. Biol. 27, 323–332. 10.1038/s41594-020-0393-9. [PubMed: 32203490]
14. Juszkiewicz S, Speldewinde SH, Wan L, Svejstrup JQ, and Hegde RS (2020). The ASC-1 Complex Disassembles Collided Ribosomes. Mol. Cell 79, 603–614.e8. 10.1016/j.molcel.2020.06.006. [PubMed: 32579943]
15. Higgins R, Gendron JM, Rising L, Mak R, Webb K, Kaiser SE, Zuzow N, Riviere P, Yang B, Fenech E, et al. (2015). The Unfolded Protein Response Triggers Site-Specific Regulatory Ubiquitylation of 40S Ribosomal Proteins. Mol. Cell 59, 35–49. 10.1016/j.molcel.2015.04.026. [PubMed: 26051182]
16. Meyer C, Garzia A, Morozov P, Molina H, and Tuschl T (2020). The G3BP1-Family-USP10 Deubiquitinase Complex Rescues Ubiquitinated 40S Subunits of Ribosomes Stalled in Translation from Lysosomal Degradation. Mol. Cell 77, 1193–1205. 10.1016/j.molcel.2019.12.024. [PubMed: 31981475]
17. Garshott DM, An H, Sundaramoorthy E, Leonard M, Vicary A, Harper JW, and Bennett EJ (2021). iRQC, a surveillance pathway for 40S ribosomal quality control during mRNA translation initiation. Cell Rep. 36, 109642. 10.1016/j.celrep.2021.109642. [PubMed: 34469731]
18. Garzia A, Meyer C, and Tuschl T (2021). The E3 ubiquitin ligase RNF10 modifies 40S ribosomal subunits of ribosomes compromised in translation. Cell Rep. 36, 109468. 10.1016/j.celrep.2021.109468. [PubMed: 34348161]
19. Pena C, Hurt E, and Panse VG (2017). Eukaryotic ribosome assembly, transport and quality control. Nat. Struct. Mol. Biol. 24, 689–699. 10.1038/nsmb.3454. [PubMed: 28880863]
20. Klinge S, and Woolford JL Jr. (2019). Ribosome assembly coming into focus. Nat. Rev. Mol. Cell Biol. 20, 116–131. 10.1038/s41580-018-0078-y. [PubMed: 30467428]
21. Broeck AV, and Klinge S (2023). Principles of Human Pre-60 S Biogenesis. Preprint at bioRxiv. 10.1101/2023.03.14.532478.
22. Dorner K, Ruggeri C, Zemp I, and Kutay U (2023). Ribosome biogenesis factors-from names to functions. EMBO J. 42, e112699. 10.15252/embj.2022112699. [PubMed: 36762427]
23. Ni C, Schmitz DA, Lee J, Paw1owski K, Wu J, and Buszczak M (2022). Labeling of heterochronic ribosomes reveals C1ORF109 and SPATA5 control a late step in human ribosome assembly. Cell Rep. 38, 110597. 10.1016/j.celrep.2022.110597. [PubMed: 35354024]

24. Helser TL, Baan RA, and Dahlberg AE (1981). Characterization of a 40S ribosomal subunit complex in polyribosomes of Saccharomyces cerevisiae treated with cycloheximide. Mol. Cell Biol. 1, 51–57. 10.1128/mcb.1.1.51-57.1981. [PubMed: 6765595]
25. Moore JB 4th, Farrar JE, Arceci RJ, Liu JM, and Ellis SR (2010). Distinct ribosome maturation defects in yeast models of Diamond-Blackfan anemia and Shwachman-Diamond syndrome. Haematologica 95, 57–64. 10.3324/haematol.2009.012450. [PubMed: 19713223]
26. Rotenberg MO, Moritz M, and Woolford JL Jr. (1988). Depletion of Saccharomyces cerevisiae ribosomal protein L16 causes a decrease in 60S ribosomal subunits and formation of half-mer polyribosomes. Genes Dev. 2, 160–172. 10.1101/gad.2.2.160. [PubMed: 3282992]
27. Ferreira-Cerca S, Kiburu I, Thomson E, LaRonde N, and Hurt E (2014). Dominant Rio1 kinase/ATPase catalytic mutant induces trapping of late pre-40S biogenesis factors in 80S-like ribosomes. Nucleic Acids Res. 42, 8635–8647. 10.1093/nar/gku542. [PubMed: 24948609]
28. Parker MD, Collins JC, Korona B, Ghalei H, and Karbstein K (2019). A kinase-dependent checkpoint prevents escape of immature ribosomes into the translating pool. PLoS Biol. 17, e3000329. 10.1371/journal.pbio.3000329. [PubMed: 31834877]
29. Lebaron S, Schneider C, van Nues RW, Swiatkowska A, Walsh D,Böttcher B, Granneman S, Watkins NJ, and Tollervey D (2012). Proofreading of pre-40S ribosome maturation by a translation initiation factor and 60S subunits. Nat. Struct. Mol. Biol. 19, 744–753. 10.1038/nsmb.2308. [PubMed: 22751017]
30. Strunk BS, Novak MN, Young CL, and Karbstein K (2012). A translation-like cycle is a quality control checkpoint for maturing 40S ribosome subunits. Cell 150, 111–121. 10.1016/j.cell.2012.04.044. [PubMed: 22770215]
31. Belhabich-Baumas K, Joret C, Jády BE, Plisson-Chastang C, Shayan R, Klopp C, Henras AK, Henry Y, and Mougin A (2017). The Rio1p ATPase hinders premature entry into translation of late pre40S pre-ribosomal particles. Nucleic Acids Res. 45, 10824–10836. 10.1093/nar/gkx734. [PubMed: 28977579]
32. Plassart L, Shayan R, Montellese C, Rinaldi D, Larburu N, Pichereaux C, Froment C, Lebaron S, O'Donohue MF, Kutay U, et al. (2021). The final step of 40S ribosomal subunit maturation is controlled by a dual key lock. Elife 10, e61254. 10.7554/eLife.61254. [PubMed: 33908345]
33. Cole SE, LaRiviere FJ, Merrikh CN, and Moore MJ (2009). A convergence of rRNA and mRNA quality control pathways revealed by mechanistic analysis of nonfunctional rRNA decay. Mol. Cell 34, 440–450. 10.1016/j.molcel.2009.04.017. [PubMed: 19481524]
34. Fujii K, Kitabatake M, Sakata T, Miyata A, and Ohno M (2009). A role for ubiquitin in the clearance of nonfunctional rRNAs. Genes Dev. 23, 963–974. 10.1101/gad.1775609. [PubMed: 19390089]
35. LaRiviere FJ, Cole SE, Ferullo DJ, and Moore MJ (2006). A late-acting quality control process for mature eukaryotic rRNAs. Mol. Cell 24, 619–626. 10.1016/j.molcel.2006.10.008. [PubMed: 17188037]
36. Sakata T, Fujii K, Ohno M, and Kitabatake M (2015). Crt10 directs the cullin-E3 ligase Rtt101 to nonfunctional 25S rRNA decay. Biochem. Biophys. Res. Commun. 457, 90–94. 10.1016/j.bbrc.2014.12.072. [PubMed: 25534857]
37. Limoncelli KA, Merrikh CN, and Moore MJ (2017). ASC1 and RPS3: new actors in 18S nonfunctional rRNA decay. RNA 23, 1946–1960. 10.1261/rna.061671.117. [PubMed: 28956756]
38. Sugiyama T, Li S, Kato M, Ikeuchi K, Ichimura A, Matsuo Y, and Inada T (2019). Sequential Ubiquitination of Ribosomal Protein uS3 Triggers the Degradation of Non-functional 18S rRNA. Cell Rep. 26, 3400–3415. 10.1016/j.celrep.2019.02.067. [PubMed: 30893611]
39. Brina D, Miluzio A, Ricciardi S, and Biffo S (2015). eIF6 anti-association activity is required for ribosome biogenesis, translational control and tumor progression. Biochim. Biophys. Acta 1849, 830–835. 10.1016/j.bbagrm.2014.09.010. [PubMed: 25252159]
40. Jaako P, Faille A, Tan S, Wong CC, Escudero-Urquijo N, Castro-Hartmann P, Wright P, Hilcenko C, Adams DJ, and Warren AJ (2022). eIF6 rebinding dynamically couples ribosome maturation and translation. Nat. Commun. 13, 1562. 10.1038/s41467-022-29214-7. [PubMed: 35322020]
41. Cheng Z, Mugler CF, Keskin A, Hodapp S, Chan LYL, Weis K, Mertins P, Regev A, Jovanovic M, and Brar GA (2019). Small and Large Ribosomal Subunit Deficiencies Lead to Distinct

Gene Expression Signatures that Reflect Cellular Growth Rate. Mol. Cell 73, 36–47. 10.1016/j.molcel.2018.10.032. [PubMed: 30503772]

42. Kappen LS, Suzuki H, and Goldberg IH (1973). Inhibition of reticulocyte peptide-chain initiation by pactamycin: accumulation of inactive ribosomal initiation complexes. Proc. Natl. Acad. Sci. USA 70, 22–26. 10.1073/pnas.70.1.22. [PubMed: 4509656]
43. Robledo S, Idol RA, Crimmins DL, Ladenson JH, Mason PJ, and Bessler M (2008). The role of human ribosomal proteins in the maturation of rRNA and ribosome production. RNA 14, 1918–1929. 10.1261/rna.1132008. [PubMed: 18697920]
44. Costa-Mattioli M, and Walter P (2020). The integrated stress response: From mechanism to disease. Science 368, eaat5314. 10.1126/science.aat5314. [PubMed: 32327570]
45. Dever TE, Ivanov IP, and Hinnebusch AG (2023). Translational regulation by uORFs and start codon selection stringency. Genes Dev. 37, 474–489. 10.1101/gad.350752.123. [PubMed: 37433636]
46. Michel AM, Fox G, M Kiran A, De Bo C, O'Connor PBF, Heaphy SM, Mullan JPA, Donohue CA, Higgins DG, and Baranov PV (2014). GWIPS-viz: development of a ribo-seq genome browser. Nucleic Acids Res. 42, D859–D864. 10.1093/nar/gkt1035. [PubMed: 24185699]
47. Ingolia NT, Brar GA, Rouskin S, McGeachy AM, and Weissman JS (2012). The ribosome profiling strategy for monitoring translation in vivo by deep sequencing of ribosome-protected mRNA fragments. Nat. Protoc. 7, 1534–1550. 10.1038/nprot.2012.086. [PubMed: 22836135]
48. Sidrauski C, McGeachy AM, Ingolia NT, and Walter P (2015). The small molecule ISRIB reverses the effects of eIF2alpha phosphorylation on translation and stress granule assembly. Elife 4, e05033. 10.7554/eLife.05033. [PubMed: 25719440]
49. Iwasaki S, Floor SN, and Ingolia NT (2016). Rocaglates convert DEAD-box protein eIF4A into a sequence-selective translational repressor. Nature 534, 558–561. 10.1038/nature17978. [PubMed: 27309803]
50. Li S, Ikeuchi K, Kato M, Buschauer R, Sugiyama T, Adachi S, Kusano H, Natsume T, Berninghausen O, Matsuo Y, et al. (2022). Sensing of individual stalled 80S ribosomes by Fap1 for nonfunctional rRNA turnover. Mol. Cell 82, 3424–3437.e8. 10.1016/j.molcel.2022.08.018. [PubMed: 36113412]
51. Khajuria RK, Munschauer M, Ulirsch JC, Fiorini C, Ludwig LS, McFarland SK, Abdulhay NJ, Specht H, Keshishian H, Mani DR, et al. (2018). Ribosome Levels Selectively Regulate Translation and Lineage Commitment in Human Hematopoiesis. Cell 173, 90–103. 10.1016/j.cell.2018.02.036. [PubMed: 29551269]
52. Wild T, Horvath P, Wyler E, Widmann B, Badertscher L, Zemp I, Kozak K, Csucs G, Lund E, and Kutay U (2010). A protein inventory of human ribosome biogenesis reveals an essential function of exportin 5 in 60S subunit export. PLoS Biol. 8, e1000522. 10.1371/journal.pbio.1000522. [PubMed: 21048991]
53. Schafer T, Strauss D, Petfalski E, Tollervey D, and Hurt E (2003). The path from nucleolar 90S to cytoplasmic 40S pre-ribosomes. EMBO J. 22, 1370–1380. 10.1093/emboj/cdg121. [PubMed: 12628929]
54. Geerlings TH, Faber AW, Bister MD, Vos JC, and Raué HA (2003). Rio2p, an evolutionarily conserved, low abundant protein kinase essential for processing of 20 S Pre-rRNA in Saccharomyces cerevisiae. J. Biol. Chem. 278, 22537–22545. 10.1074/jbc.M300759200. [PubMed: 12690111]
55. Vanrobays E, Gelugne JP, Gleizes PE, and Caizergues-Ferrer M(2003). Late cytoplasmic maturation of the small ribosomal subunit requires RIO proteins in Saccharomyces cerevisiae. Mol. Cell Biol. 23, 2083–2095. 10.1128/MCB.23.6.2083-2095.2003. [PubMed: 12612080]
56. Vanrobays E, Gleizes PE, Bousquet-Antonelli C, Noaillac-Depeyre J,Caizergues-Ferrer M, and Gélugne JP (2001). Processing of 20S prerRNA to 18S ribosomal RNA in yeast requires Rrp10p, an essential non-ribosomal cytoplasmic protein. EMBO J. 20, 4204–4213. 10.1093/emboj/20.15.4204. [PubMed: 11483523]
57. Widmann B, Wandrey F, Badertscher L, Wyler E, Pfannstiel J, Zemp I, and Kutay U (2012). The kinase activity of human Rio1 is required for final steps of cytoplasmic maturation of 40S subunits. Mol. Biol. Cell 23, 22–35. 10.1091/mbc.E11-07-0639. [PubMed: 22072790]

58. Rouquette J, Choesmel V, and Gleizes PE (2005). Nuclear export and cytoplasmic processing of precursors to the 40S ribosomal subunits in mammalian cells. EMBO J. 24, 2862–2872. 10.1038/sj.emboj.7600752. [PubMed: 16037817]
59. LaRonde-LeBlanc N, and Wlodawer A (2005). The RIO kinases: an atypical protein kinase family required for ribosome biogenesis and cell cycle progression. Biochim. Biophys. Acta 1754, 14–24. 10.1016/j.bbapap.2005.07.037. [PubMed: 16182620]
60. Fenner BJ, Scannell M, and Prehn JHM (2009). Identification of polyubiquitin binding proteins involved in NF-kappaB signaling using protein arrays. Biochim. Biophys. Acta 1794, 1010–1016. 10.1016/j.bbapap.2009.02.013. [PubMed: 19285159]
61. Penengo L, Mapelli M, Murachelli AG, Confalonieri S, Magri L, Musacchio A, Di Fiore PP, Polo S, and Schneider TR (2006). Crystal structure of the ubiquitin binding domains of rabex-5 reveals two modes of interaction with ubiquitin. Cell 124, 1183–1195. 10.1016/j.cell.2006.02.020. [PubMed: 16499958]
62. Lee S, Tsai YC, Mattera R, Smith WJ, Kostelansky MS, Weissman AM, Bonifacino JS, and Hurley JH (2006). Structural basis for ubiquitin recognition and autoubiquitination by Rabex-5. Nat. Struct. Mol. Biol. 13, 264–271. 10.1038/nsmb1064. [PubMed: 16462746]
63. Kristariyanto YA, Abdul Rehman SA, Weidlich S, Knebel A, and Kulathu Y (2017). A single MIU motif of MINDY-1 recognizes K48-linked polyubiquitin chains. EMBO Rep. 18, 392–402. 10.15252/embr.201643205. [PubMed: 28082312]
64. Lehmann JA, Lindner D, Sung HM, and Stoecklin G (2024). E3 ubiquitin ligase RNF10 promotes dissociation of stalled ribosomes and responds to ribosomal subunit imbalance. Nat. Commun. 15, 10350. 10.1038/s41467-024-54411-x. [PubMed: 39609413]
65. Harding HP, Ordonez A, Allen F, Parts L, Inglis AJ, Williams RL, and Ron D (2019). The ribosomal P-stalk couples amino acid starvation to GCN2 activation in mammalian cells. Elife 8, e50149. 10.7554/eLife.50149. [PubMed: 31749445]
66. Ford PW, Narasimhan M, and Bennett EJ (2024). Ubiquitin-dependent translation control mechanisms: Degradation and beyond. Cell Rep. 43, 115050. 10.1016/j.celrep.2024.115050. [PubMed: 39661518]
67. Zhao S, Cordes J, Caban KM, Götz MJ, Mackens-Kiani T, Veltri AJ, Sinha NK, Weickert P, Kaya S, Hewitt G, et al. (2023). RNF14-dependent atypical ubiquitylation promotes translation-coupled resolution of RNA-protein crosslinks. Mol. Cell 83, 4290–4303. 10.1016/j.molcel.2023.10.012. [PubMed: 37951216]
68. Wu CCC, Peterson A, Zinshteyn B, Regot S, and Green R (2020). Ribosome Collisions Trigger General Stress Responses to Regulate Cell Fate. Cell 182, 404–416. 10.1016/j.cell.2020.06.006. [PubMed: 32610081]
69. Farley-Barnes KI, Ogawa LM, and Baserga SJ (2019). Ribosomopathies: Old Concepts, New Controversies. Trends Genet. 35, 754–767. 10.1016/j.tig.2019.07.004. [PubMed: 31376929]
70. Mirabello L, Khincha PP, Ellis SR, Giri N, Brodie S, Chandrasekharappa SC, Donovan FX, Zhou W, Hicks BD, Boland JF, et al. (2017). Novel and known ribosomal causes of Diamond-Blackfan anaemia identified through comprehensive genomic characterisation. J. Med. Genet. 54, 417–425. 10.1136/jmedgenet-2016-104346. [PubMed: 28280134]
71. An H, Ordureau A, Körner M, Paulo JA, and Harper JW (2020). Systematic quantitative analysis of ribosome inventory during nutrient stress. Nature 583, 303–309. 10.1038/s41586-020-2446-y. [PubMed: 32612236]
72. Miscicka A, Bulakhov AG, Kuroha K, Zinoviev A, Hellen CUT, and Pestova TV (2024). Ribosomal collision is not a prerequisite for ZNF598-mediated ribosome ubiquitination and disassembly of ribosomal complexes by ASCC. Nucleic Acids Res. 52, 4627–4643. 10.1093/nar/gkae087. [PubMed: 38366554]
73. Montellese C, van den Heuvel J, Ashiono C, Dörner K, Melnik A, Jonas S, Zemp I, Picotti P, Gillet LC, and Kutay U (2020). USP16 counteracts mono-ubiquitination of RPS27a and promotes maturation of the 40S ribosomal subunit. Elife 9, e54435. 10.7554/eLife.54435. [PubMed: 32129764]

74. Parker MD, Brunk ES, Getzler AJ, and Karbstein K (2024). The kinase Rio1 and a ribosome collision-dependent decay pathway survey the integrity of 18S rRNA cleavage. PLoS Biol. 22, e3001767. 10.1371/journal.pbio.3001767. [PubMed: 39038273]

75. Skowronek P, Thielert M, Voytik E, Tanzer MC, Hansen FM, Willems S, Karayel O, Brunner AD, Meier F, and Mann M (2022). Rapid and In-Depth Coverage of the (Phospho-)Proteome With Deep Libraries and Optimal Window Design for dia-PASEF. Mol. Cell. Proteomics 21, 100279. 10.1016/j.mcpro.2022.100279. [PubMed: 35944843]

76. Demichev V, Messner CB, Vernardis SI, Lilley KS, and Ralser M (2020). DIA-NN: neural networks and interference correction enable deep proteome coverage in high throughput. Nat. Methods 17, 41–44. 10.1038/s41592-019-0638-x. [PubMed: 31768060]

77. Yang X, Boehm JS, Yang X, Salehi-Ashtiani K, Hao T, Shen Y, Lubonja R, Thomas SR, Alkan O, Bhimdi T, et al. (2011). A public genome-scale lentiviral expression library of human ORFs. Nat. Methods 8, 659–661. 10.1038/nmeth.1638. [PubMed: 21706014]

78. Ritchie ME, Phipson B, Wu D, Hu Y, Law CW, Shi W, and Smyth GK (2015). limma powers differential expression analyses for RNA-sequencing and microarray studies. Nucleic Acids Res. 43, e47. 10.1093/nar/gkv007. [PubMed: 25605792]

79. Johnson AG, Flynn RA, Lapointe CP, Ooi YS, Zhao ML, Richards CM, Qiao W, Yamada SB, Couthouis J, Gitler AD, et al. (2020). A memory of eS25 loss drives resistance phenotypes. Nucleic Acids Res. 48, 7279–7297. 10.1093/nar/gkaa444. [PubMed: 32463448]

Highlights

- Depletion of 60S subunits or amino acid starvation activates the iRQC pathway
- RNF10 expression is regulated via a translation control mechanism utilizing conserved uORFs
- RNF10 acts on 40S subunits engaged with mRNA
- RIOK3 ubiquitin binding and kinase activity are required for iRQC-mediated 40S degradation

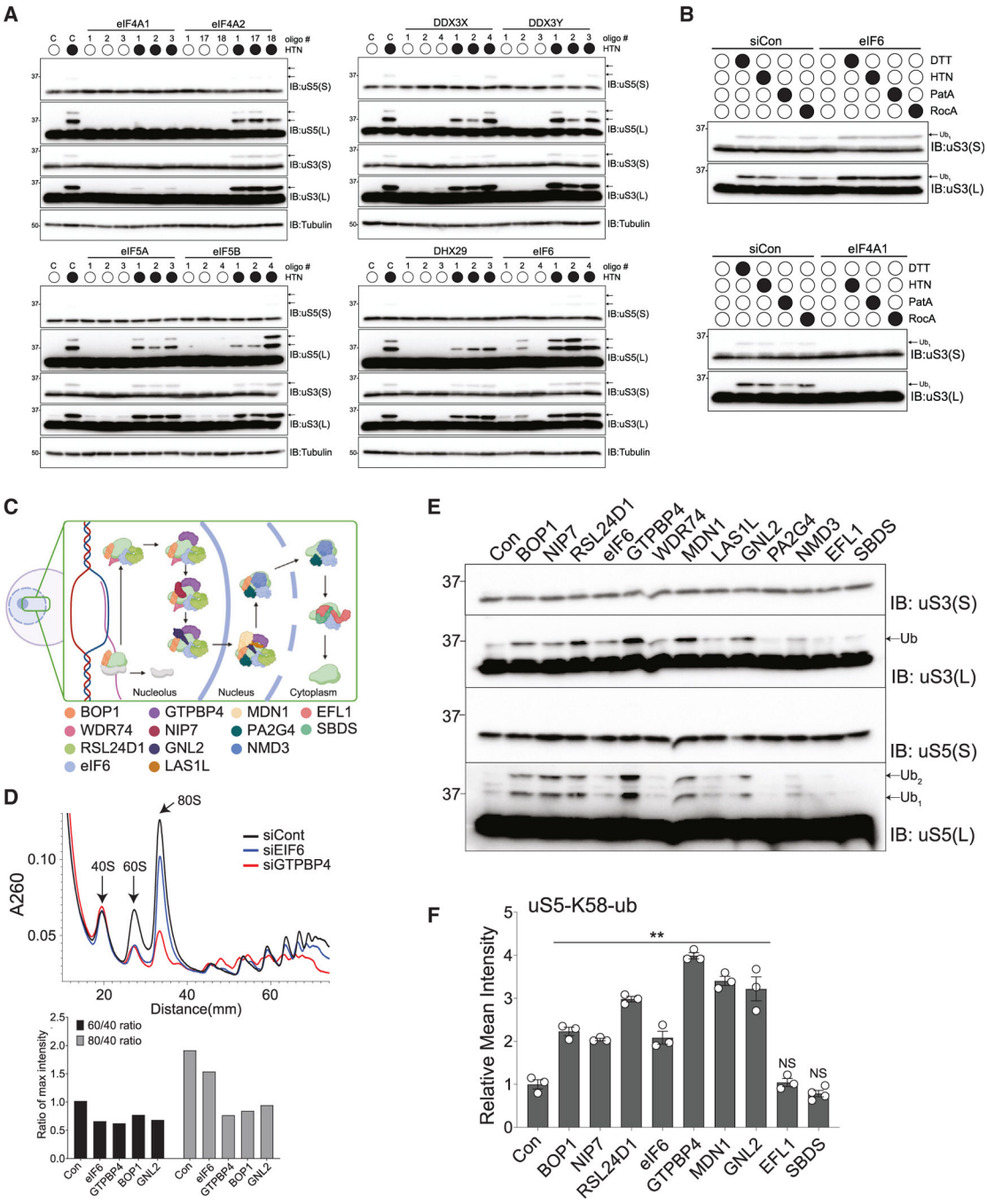

Figure 1. Impairing 60S biogenesis stimulates ribosome ubiquitylation

(A) 293T cells transfected with non-targeting siRNA (siCon) or three independent siRNA oligonucleotides targeting the indicated translation factor were either untreated or treated with harringtonine (HTN) for 2 h. Whole-cell extracts were analyzed by SDS-PAGE followed by immunoblotting with antibodies against uS3 and uS5. The ubiquitin-modified uS3 and uS5 are indicated by the arrows. S, short exposure; L, long exposure.

(B) 293T cells transfected with control siRNA or siRNAs targeting EIF4A1 or EIF6 were either untreated or treated with the indicated inhibitors for 2 h. Whole-cell extracts were

analyzed by SDS-PAGE followed by immunoblotting with antibodies against uS3. The ubiquitin-modified uS3 is indicated by the arrows. S, short exposure; L, long exposure.
(C) Schematic representation of ribosome biogenesis pathways with targeted 60S biogenesis factors indicated.
(D) Whole-cell extracts from 293 Flp-In cells transfected with non-targeting or 60S-biogenesis-factor-targeting siRNAs were fractionated on sucrose gradients.40S, 60S, and 80S peaks are as indicated. (Top) Absorbance at 260 nm indicating ribosomal abundance across the gradient. (Bottom) The 60S:40S and 80S:40S ratio upon knockdown of the indicated 60S biogenesis factor as calculated from the sucrose gradient absorbance profile.
(E) Whole-cell extracts from 293T cells transfected with siRNAs targeting the indicated 60S biogenesis factor were immunoblotted with antibodies against uS3 and uS5. The ubiquitin-modified uS3 and uS5 are indicated by the arrows. S, short exposure; L, long exposure.
(F) Ubiquitylated uS5-K58 peptide intensity quantified by mass spectrometry from 293T cells transfected with non-targeting siRNA or siRNAs targeting indicated biogenesis factors. n = 3, error bars indicate SEM; **p < 0.01 by Student's t test.

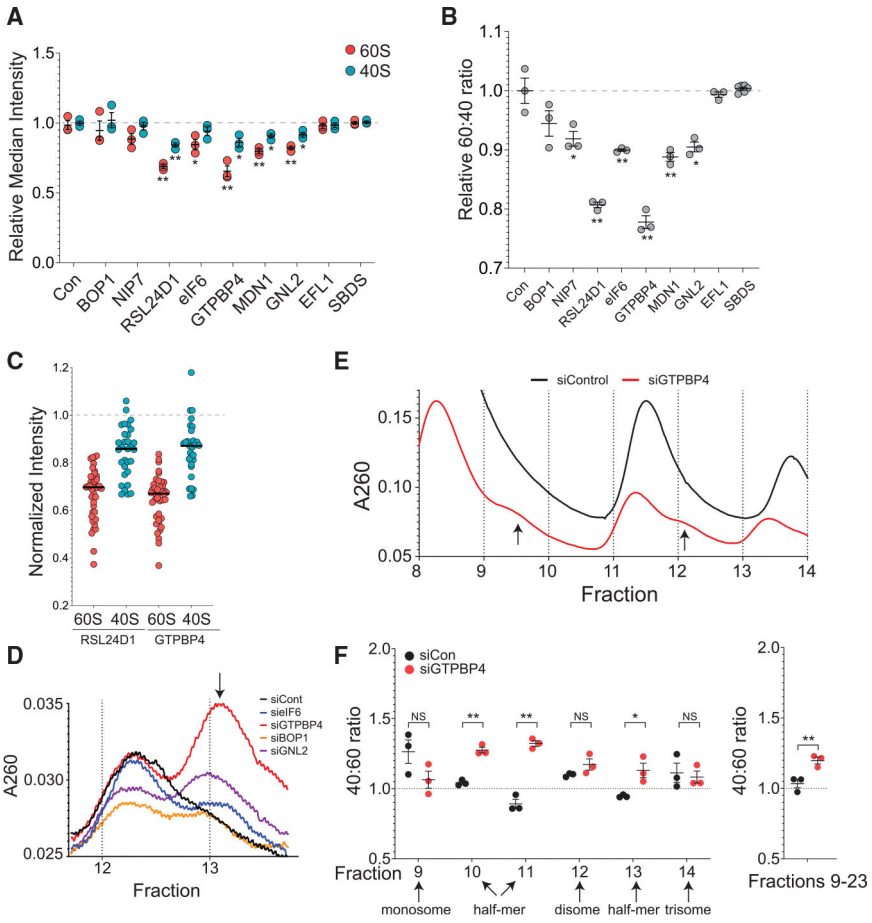

Figure 2. Disruption of 60S biogenesis results in a concomitant reduction in 40S levels, and excess 40S subunits are translationally active

(A) Relative median intensity of all 60S and 40S proteins as quantified by mass spectrometry in 293T cells transfected with the indicated siRNA.

(B) Relative ratio of the summed intensity of 60S proteins to 40S proteins as quantified by mass spectrometry in 293T cells transfected with the indicated siRNA.

(C) Normalized intensity of individual 40S and 60S proteins in 293T cells transfected with the indicated siRNA. The median protein intensity is indicated by the black bar.

(D) Enhanced view of disome-containing sucrose gradient fractions from 293 Flp-In cells after knockdown of the indicated genes. Absorbance curves were aligned based on the local maximum of the disome peak. Fraction numbers indicate collections from siControl. Disome-associated half-mer peak is indicated by the arrow.

(E) Representative 260 nm absorbance from selected sucrose gradient fractions for whole-cell extracts from 293 Flp-In cells transfected with non-targeting or GTPBP4-targeting siRNA. Half-mer peaks are indicated by arrows.

(F) Relative ratio of the median 40S to 60S protein intensity as quantified by mass spectrometry in the indicated sucrose gradient fractions. For (A)–(F), $n = 3$, error bars indicate SEM; *$p < 0.05$ and **$p < 0.01$ by Student's t test.

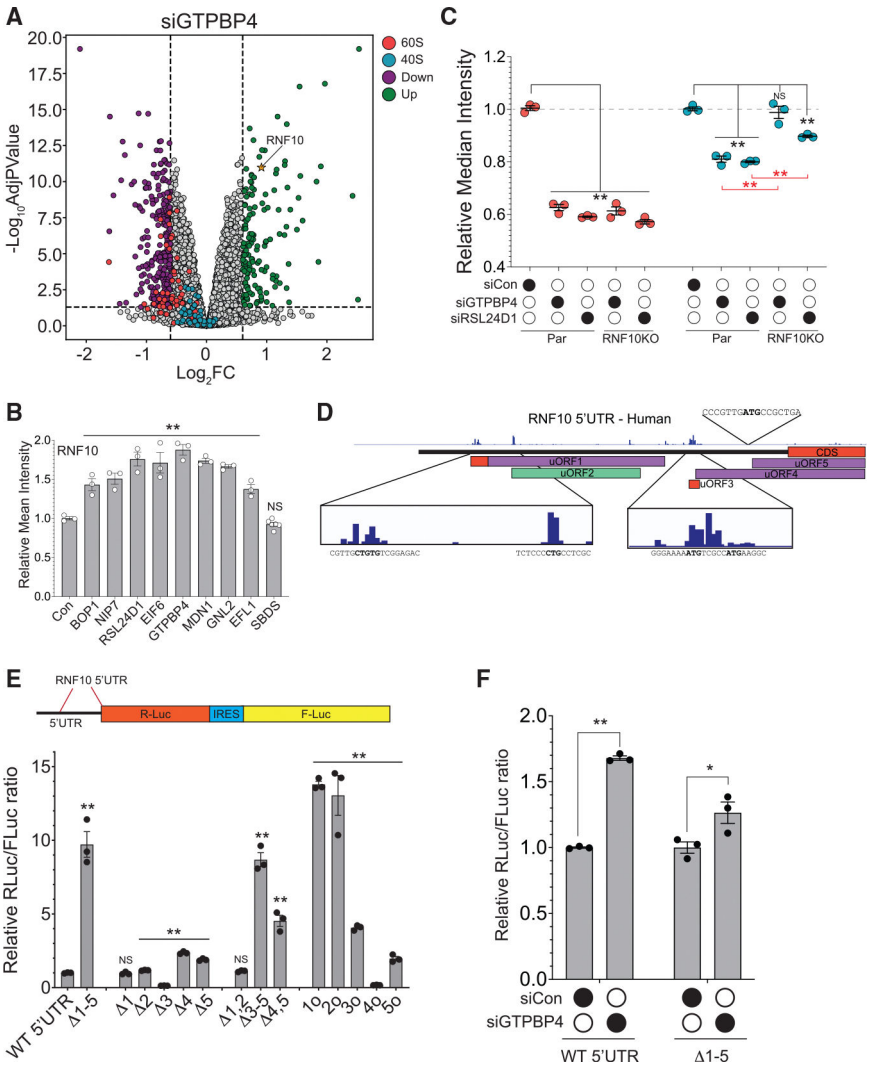

Figure 3. RNF10 is required for 40S decay and is post-transcriptionally upregulated in response to 60S biogenesis disruption

(A) Volcano plot showing differentially expressed proteins between 293T cells transfected with GTPBP4- or control-targeting siRNA. Proteins with an absolute $\log_2$ fold change >0.6 and a negative $\log_{10}$ adjusted $p > 1.3$ are colored as indicated.

(B) Relative mean intensity of RNF10 protein as quantified by mass spectrometry in 293T cells transfected with non-targeting (Con) or 60S-biogenesis-factor-targeting siRNA as indicated.

(C) Relative median intensity of 60S and 40S proteins, normalized to siCon quantified by mass spectrometry in 293 Flp-In parental or RNF10 KO cells transfected with the indicated siRNA.

(D) Schematic of the RNF10 5′ UTR with ribosome occupancy from RiboSeq data. Five putative uORFs are outlined by boxes; color indicates the reading frame of each uORF. uORF start locations and their sequence context are annotated below the corresponding tracks.

(E) Top, schematic of the dual luciferase reporter. Bottom, Rluc:Fluc ratio relative to the WT RNF10 5′ UTR reporter of cells transfected with the indicated RNF10 5′ UTR reporters. (F) Rluc:Fluc ratio relative to siCon for cells co-transfected with either the WT RNF10 5′ UTR reporter or the 5′ UTR reporter lacking all five uORF start codons and GTPBP4-targeting siRNA. For (A)–(F), $n = 3$, error bars indicate SEM; NS, not significant; *$p < 0.05$ and **$p < 0.01$ by Student's t test. Red lines or asterisks indicate a comparison to knockdown of 60S biogenesis alone.

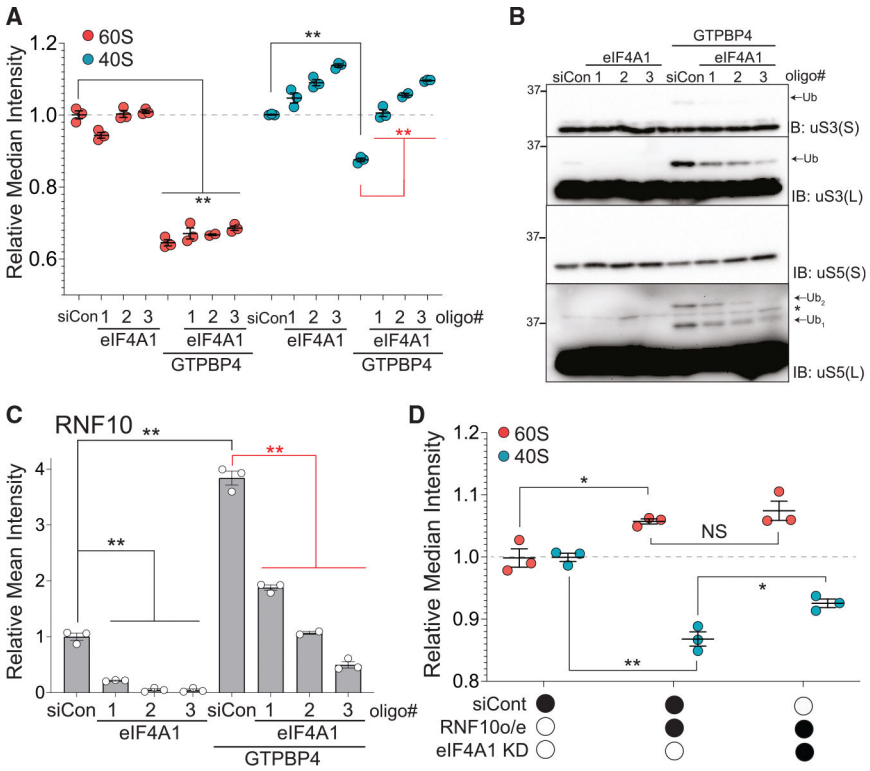

Figure 4. RNF10-mediated ribosomal ubiquitylation and 40S decay requires EIF4A1

(A) Relative median intensity of 60S and 40S proteins, normalized to siCon, as quantified by mass spectrometry in 293 Flp-In cells transfected with siCon or siRNAs targeting either GTPBP4 or EIF4A1 or both GTPBP4 and eIF4A1 as indicated.

(B) Whole-cell extracts from 293 Flp-In cells transfected with siRNA targeting GTPBP4 and/or EIF4A1 as indicated were immunoblotted with antibodies against uS3 and uS5. The ubiquitin-modified uS3 and uS5 are indicated by the arrows. S, short exposure; L, long exposure. * indicates a non-specific band.

(C) Relative mean intensity of RNF10 protein as quantified by mass spectrometry in 293T cells transfected with non-targeting siRNAs or siRNAs targeting either GTPBP4 or EIF4A1 or both GTPBP4 and EIF4A1 as indicated.

(D) Relative median intensity of 60S and 40S proteins, normalized to siCon as quantified by mass spectrometry in 293 Flp-In cells transfected with non-targeting siRNA (siCon) or EIF4A1-targeting siRNA and with or without induction of RNF10 overexpression as indicated.

For (A)–(D), $n = 3$, error bars indicate SEM; *$p < 0.05$ and **$p < 0.01$ by Student's t test. Red lines, text, or asterisks indicate a comparison to siGTPBP4 alone.

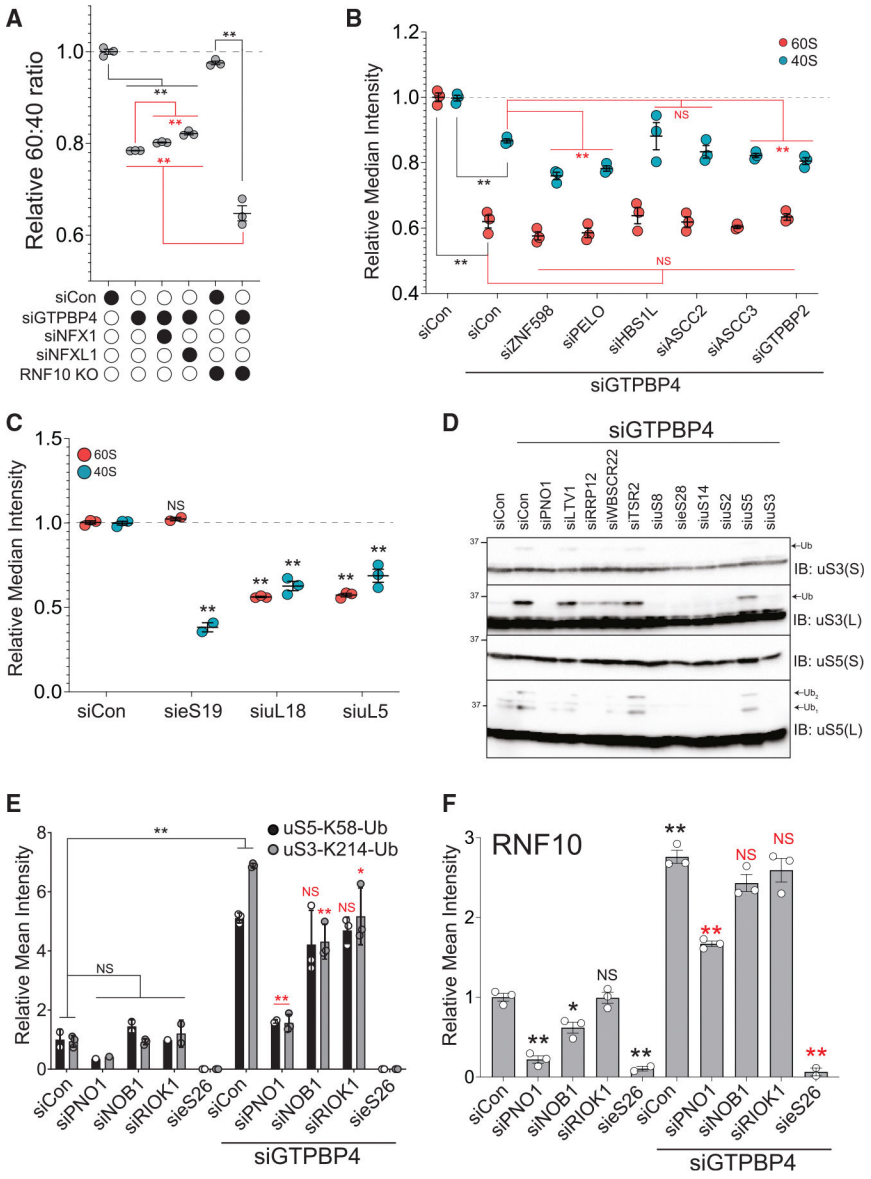

Figure 5. 60S:40S subunit imbalance activates iRQC

(A) Relative ratio of the summed intensity of 60S proteins to 40S proteins as quantified by mass spectrometry in 293 Flp-In cells transfected with siCon or siRNAs targeting GTPBP4 and NFX1 or NFXL1 as indicated.

(B) Relative median intensity of 60S and 40S proteins, normalized to non-targeting siRNA, as quantified by mass spectrometry in 293 Flp-In cells transfected with siCon or siRNAs targeting GTPBP4 and the indicated RQC factors.

(C) Relative median intensity of 60S and 40S proteins, normalized to siCon, as quantified by mass spectrometry in 293 Flp-In cells transfected with siCon or siRNAs targeting the indicated ribosomal proteins.

(D) Whole-cell extracts from 293T cells transfected with siRNA targeting GTPBP4 and either non-targeting (siCon) siRNA or siRNAs targeting the indicated 40S biogenesis factor

or 40S protein were immunoblotted with antibodies against uS3 and uS5. The ubiquitin-modified uS3 and uS5 are indicated by the arrows. S, short exposure; L, long exposure.
(E) Ubiquitylated uS5-K58 and uS3-K214 peptide intensity quantified by mass spectrometry from 293 Flp-In cells transfected with siCon or siRNAs targeting the indicated 40S biogenesis factor or 40S protein with or without GTPBP4-targeting siRNA.
(F) Relative mean intensity of RNF10 protein as quantified by mass spectrometry in 293 Flp-In cells transfected with siCon or siRNAs targeting the indicated factor.
For (A)–(F), $n = 3$, error bars indicate SEM; NS, not significant; *$p < 0.05$ and **$p < 0.01$ by Student's t test. Red lines, text, or asterisks indicate a comparison to siGTPBP4 alone.

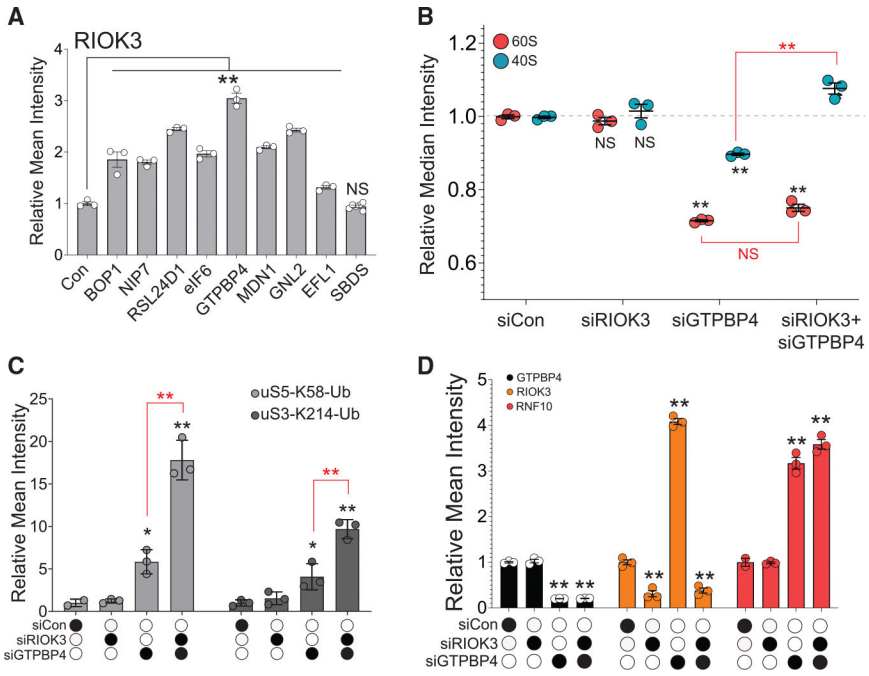

Figure 6. RIOK3 is required for RNF10-dependent 40S decay

(A) Relative mean intensity of RIOK3 protein as quantified by mass spectrometry in 293T cells transfected with non-targeting (Con) or 60S-biogenesis-factor-targeting siRNA as indicated.

(B) Relative median intensity of 60S and 40S proteins, normalized to non-targeting siRNA, as quantified by mass spectrometry in 293 Flp-In cells transfected with siCon or siRNAs targeting GTPBP4 or RIOK3.

(C) Ubiquitylated uS5-K58 and uS3-K214 peptide intensity quantified by mass spectrometry from 293 Flp-In cells transfected with siCon or siRNAs targeting GTPBP4 or RIOK3 as indicated.

(D) Relative mean intensity of indicated proteins as quantified by mass spectrometry in 293 Flp-In cells transfected with siCon or siRNAs targeting GTPBP4 or RIOK3 as indicated.

For (A)–(D), $n = 3$, error bars indicate SEM; NS, not significant; $*p < 0.05$ and $**p < 0.01$ by Student's t test. Red lines, text, or asterisks indicate a comparison to siGTPBP4 alone.

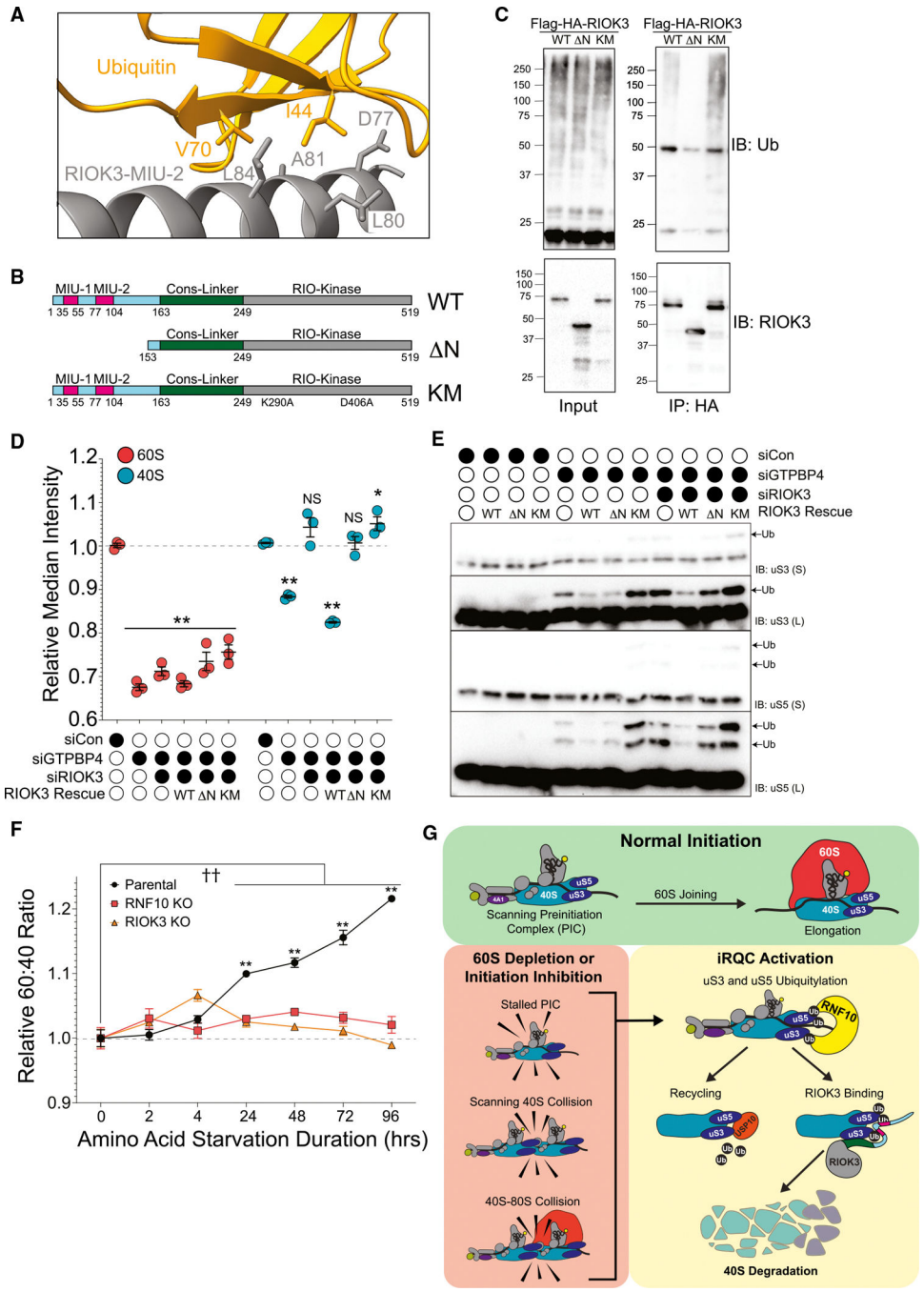

Figure 7. RIOK3 ubiquitin binding is necessary to facilitate 40S degradation upon iRQC pathway activation

(A) AlphaFold 3 model with RIOK3 MIU-2 domain (gray) and ubiquitin (orange). MIU domain residues (gray text) and ubiquitin residues (orange text) at the putative interaction surface are indicated.

(B) Schematics of RIOK3 WT, ΔN, and KM constructs.

(C) FLAG-hemagglutinin (HA)-tagged RIOK3 was immunoprecipitated from cell lines with stable expression of wild-type or mutant RIOK3. Whole-cell extracts and HA immunoprecipitates were immunoblotted with antibodies as indicated.

(D) Relative median intensity of 60S and 40S proteins, normalized to non-targeting siRNA, as quantified by mass spectrometry from parental or RIOK3 stably expressing lines transfected with siRNAs targeting GTPBP4 or RIOK3 as indicated. RIOK3 transgenes are resistant to RIOK3 siRNA. n = 3, error bars indicate SEM; NS, not significant; *$p < 0.05$ and **$p < 0.01$ by Student's t test.

(E) Whole-cell extracts from parental or RIOK3 variant stably expressing lines transfected with siRNAs targeting GTPBP4 or RIOK3 or not targeting (siCon), as indicated, were immunoblotted with antibodies against uS3 and uS5. The ubiquitin-modified uS3 and uS5 are indicated by the arrows. S, short exposure; L, long exposure.

(F) Relative 60:40 summed protein abundance ratio as quantified by mass spectrometry from parental 293 Flp-In cells (black line/circles), RNF10-KO cells(red line/boxes), or RIOK3-KO cells (orange line/triangles) cultured in lysine- and arginine-free medium for the indicated time. $n = 3$, error bars indicate SEM; **$p < 0.01$ by Tukey's HSD test comparing parental to both RNF10-KO and RIOK3-KO cell lines. ††$p < 0.01$ by Dunnett's test comparing the zero time point for the cell line indicated by color.

(G) Model for RNF10- and RIOK3-mediated 40S decay.

KEY RESOURCES TABLE

REAGENT or RESOURCE	SOURCE	IDENTIFIER
Antibodies		
Rabbit monoclonal anti-RPS3 (uS3)	Bethyl Laboratories	Cat# A303-840A; RRID:AB_2615588
Rabbit monoclonal anti-RPS2 (uS5)	Bethyl Laboratories	Cat# A303-794A; RRID:AB_11218192
Mouse monoclonal a-Tubulin	Cell Signaling Technology	Cat# 3873, RRID:AB_1904178
Rabbit polyclonal anti-eIF4A1	Cell Signaling Technology	Cat# 2490; RRID:AB_823487
Rabbit monoclonal anti-eIF6	Cell Signaling Technology	Cat# 3833; RRID: AB_2096520
Mouse monoclonal anti-Puromycin	Millipore	Cat# MABE343, RRID:AB_2566826
Rabbit polyclonal anti-SBDS	GeneTex	Cat# GTX109168; RRID:AB_1951814
Mouse monoclonal anti-Ubiquitin	Millipore	Cat# MAB1510; RRID:AB_2180556
Rabbit polyclonal anti-RIOK3	Bethyl Laboratories	Cat# A305-602A; RRID:AB_2891516
Anti-Rabbit IgG (H+L), HRP Conjugate antibody	Promega	Cat# W4011; RRID:AB_430833
Anti-Mouse IgG (H+L) HRP Conjugate antibody	Promega	Cat# W4021; RRID:AB_430834
Chemicals, peptides, and recombinant proteins		
DMEM, high glucose, pyruvate	Thermo Fisher Scientific	Cat# 11995065
IMDM	Thermo Fisher Scientific	Cat# 12440053
RPMI	Thermo Fisher Scientific	Cat# SH30027FS
DMEM for SILAC	Thermo Fisher Scientific	Cat# 88364
Fetal Bovine Serum	Sigma-Aldrich	Cat# F2442
Opti-MEM	Thermo Fisher Scientific	Cat# 31985070
Lipofectamine RNAiMax	Thermo Fisher Scientific	Cat# 13778030
Lipofectamine 2000	Thermo Fisher Scientific	Cat# 11668019
Lipofectamine 3000	Thermo Fisher Scientific	Cat# L3000001
TransIT 293	Mirus Bio LLC	Cat# MIR 2700
Harringtonine (HTN)	LKT labs	Cat# H0169
Dithiothreitol (DTT)	Fisher	Cat# BP172-25
PatamineA (PatA)	Gift from Jeremy Pelletier's lab	N/A
Rocaglamide (RocA)	MedChemExpress	Cat# HY19256
Protease inhibitor cocktail tablet	Roche	Cat# 11836170001
N-Ethylmaleimide (NEM)	Sigma-Aldrich	Cat# E3876
2-mercaptoethanol	J.T. Baker	Cat# 4049-00
Clarity Western ECL Substrate	BioRad	Cat# 170-5061
Puromycin	Corning	Cat# 61-385-RA
Cycloheximide	MP Biomedicals	Cat# 100183
Iodoacetamide (IAA)	MP Biomedicals	Cat# 100351
Lys-C	FUJIFILM Wako Pure Chemical Corporation	Cat# 21-05063
Trypsin	Promega	Cat# V5111
Triton X-100	Sigma	Cat# T8787
Turbo DNase	Invitrogen	Cat# AM2238

REAGENT or RESOURCE	SOURCE	IDENTIFIER
SUPERase-In	Invitrogen	Cat# AM2696
Trichloroacetic Acid (TCA)	Sigma	Cat# T0699
TRIzol	Life Technologies	Cat# 1596026
Super-Script III First-Strand Synthesis System	Life Technologies	Cat# 18080051
iTaq Universal SYBR Green Supermix	BioRad	Cat# 1725121
Doxycycline hydrochloride	Fisher Scientific	Cat# BP2653-5
Critical commercial assays		
BCA Protein Assay	Thermo Scientific (Pierce)	Cat# 23225
CellTiter-Glo 2.0 Cell Viability Assay	Promega	Cat# G9243
Dual-Glo Luciferase Assay System	Promega	Cat# E2940
Deposited data		
60S biogenesis knockdown proteomics (S3A–S3D, Figures 1F and 2A–C, 3A–3C, 6A; S1F; S2A)	This paper	PRIDE: PXD060355
Sucrose gradient siGTPBP4 proteomics (Figure 2F)	This paper	PRIDE: PXD060349
RNF10 KO with 60S biogenesis knockdown proteomics (Figures 3C and 5A, S3F–S3G, S6A)	This paper	PRIDE: PXD060309
eIF4A1 and GTPBP4 co-knockdown proteomics (Figures 4A and 4C; S4A)	This paper	PRIDE: PXD060375
RNF10 OE with eIF4A1 knockdown proteomics (Figures 4D, S4D)	This paper	PRIDE: PXD060334
GTPBP4 and NFX1/NFXL1 co-knockdown proteomics (Figures 5A, S5A–S5B)	This paper	PRIDE: PXD060331
eRQC factors and GTPBP4 co-knockdown proteomics (Figure 5B, S5C–S5E)	This paper	PRIDE: PXD060206
DBA-related proteins knockdown proteomics (Figures 5C, S5F)	This paper	PRIDE: PXD060207
40S biogenesis factor and GTPBP4 co-knockdown proteomics (Figures 5E–5F, S5G–S5H)	This paper	PRIDE: PXD060296
eS26 (RPS26) and GTPBP4 co-knockdown proteomics (Figures 5E–5F, S5G–S5H)	This paper	PRIDE: PXD060177
RIOK3 and GTPBP4 co-knockdown proteomics (Figures 6B–6D)	This paper	PRIDE: PXD060208
RNF10 OE proteomics (Figure S6B)	This paper	PRIDE: PXD060299
RIOK3 KO with GTPBP4 knockdown proteomics (Figures S6C–S6D)	This paper	PRIDE: PXD060294
RIOK3 variants rescue proteomics (Figures 7D, S7G)	This paper	PRIDE: PXD060301
Amino acid starvation in RNF10 KO and RIOK3 KO cell lines proteomics (Figure 7F, S7E–S7F, S7H–S7I)	This paper	PRIDE: PXD060308
Experimental models: Cell lines		
HEK293T	ATCC	Cat# CRL-3216
293Flp-In T-REx	Thermo Fisher Scientific	Cat# R78007
HAP1	Johnson et al.[79]	N/A
OVTOKO	JCRB Cell Bank	Cat# JCRB1048
293FlpIn-RNF10KO	Garshott et al.[17]	N/A

REAGENT or RESOURCE	SOURCE	IDENTIFIER
293FlpIn-FRT-Flag-HA-RNF10wt	Garshott et al.[17]	N/A
293FlpIn-RIOK3KO_C4	This paper	N/A
293FlpIn-Flag-HA-RIOK3-WT-siRes	This paper	N/A
293FlpIn-Flag-HA-RIOK3-ΔN-siRes	This paper	N/A
293FlpIn-Flag-HA-RIOK3-KM-siRes	This paper	N/A
Oligonucleotides		
For oligonucleotides, see Table S1	N/A	N/A
Recombinant DNA		
pcDNA3-RLUC-IRES-FLUC	Addgene	Cat# 45642
pDONR-RIOK3-CDS	hORFeome V8.1; Yang et al.[77]	N/A
pSpCas9(BB)-2a-GFP plasmid (PX458)	Addgene	Cat# 48138
pcDNA3-RNF10-WT-UTR-RLUC-IRES-FLUC	This paper	N/A
pcDNA3-RNF10-UTR-Start_1_mut-RLUC-IRES-FLUC	This paper	N/A
pcDNA3-RNF10-UTR-Start_2_mut-RLUC-IRES-FLUC	This paper	N/A
pcDNA3-RNF10-UTR-Start_3_mut-RLUC-IRES-FLUC	This paper	N/A
pcDNA3-RNF10-UTR-Start_4_mut-RLUC-IRES-FLUC	This paper	N/A
pcDNA3-RNF10-UTR-Start_5_mut-RLUC-IRES-FLUC	This paper	N/A
pcDNA3-RNF10-UTR-Start_1,2_mut-RLUC-IRES-FLUC	This paper	N/A
pcDNA3-RNF10-UTR-Start_1,3_mut-RLUC-IRES-FLUC	This paper	N/A
pcDNA3-RNF10-UTR-Start_1,4_mut-RLUC-IRES-FLUC	This paper	N/A
pcDNA3-RNF10-UTR-Start_1,5_mut-RLUC-IRES-FLUC	This paper	N/A
pcDNA3-RNF10-UTR-Start_2,3_mut-RLUC-IRES-FLUC	This paper	N/A
pcDNA3-RNF10-UTR-Start_2,4_mut-RLUC-IRES-FLUC	This paper	N/A
pcDNA3-RNF10-UTR-Start_2,5_mut-RLUC-IRES-FLUC	This paper	N/A
pcDNA3-RNF10-UTR-Start_3,4_mut-RLUC-IRES-FLUC	This paper	N/A
pcDNA3-RNF10-UTR-Start_3,5_mut-RLUC-IRES-FLUC	This paper	N/A
pcDNA3-RNF10-UTR-Start_4,5_mut-RLUC-IRES-FLUC	This paper	N/A
pcDNA3-RNF10-UTR-Start_1,2,3_mut-RLUC-IRES-FLUC	This paper	N/A
pcDNA3-RNF10-UTR-Start_1,2,4_mut-RLUC-IRES-FLUC	This paper	N/A
pcDNA3-RNF10-UTR-Start_1,2,5_mut-RLUC-IRES-FLUC	This paper	N/A
pcDNA3-RNF10-UTR-Start_1,3,4_mut-RLUC-IRES-FLUC	This paper	N/A
pcDNA3-RNF10-UTR-Start_1,3,5_mut-RLUC-IRES-FLUC	This paper	N/A
pcDNA3-RNF10-UTR-Start_1,4,5_mut-RLUC-IRES-FLUC	This paper	N/A
pcDNA3-RNF10-UTR-Start_2,3,4_mut-RLUC-IRES-FLUC	This paper	N/A
pcDNA3-RNF10-UTR-Start_2,3,5_mut-RLUC-IRES-FLUC	This paper	N/A
pcDNA3-RNF10-UTR-Start_2,4,5_mut-RLUC-IRES-FLUC	This paper	N/A
pcDNA3-RNF10-UTR-Start_3,4,5_mut-RLUC-IRES-FLUC	This paper	N/A
pcDNA3-RNF10-UTR-Start_1,2,3,4_mut-RLUC-IRES-FLUC	This paper	N/A

REAGENT or RESOURCE	SOURCE	IDENTIFIER
pcDNA3-RNF10-UTR-Start_1,2,3,5_mut-RLUC-IRES-FLUC	This paper	N/A
pcDNA3-RNF10-UTR-Start_1,2,4,5_mut-RLUC-IRES-FLUC	This paper	N/A
pcDNA3-RNF10-UTR-Start_1,3,4,5_mut-RLUC-IRES-FLUC	This paper	N/A
pcDNA3-RNF10-UTR-Start_2,3,4,5_mut-RLUC-IRES-FLUC	This paper	N/A
pcDNA3-RNF10-UTR-Start_1,2,3,4,5_mut-RLUC-IRES-FLUC	This paper	N/A
PX458-RIOK3-gRNA	This paper	N/A
pHAGE-NTAP-RIOK3-WT-siRes	This paper	N/A
pHAGE-NTAP-RIOK3-ΔN-siRes	This paper	N/A
pHAGE-NTAP-RIOK3-KM-siRes	This paper	N/A
Software and algorithms		
Bio-Rad Image Lab software	BioRad	Cat# 12012931; RRID:SCR_014210
GloMax®-96 Software v1.9.3	Promega	RRID:SCR_026323
py_diAID	Skowronek et al.[75]	RRID:SCR_025304
DIA-NN	Demichev et al.[76]	RRID:SCR_022865
GraphPad Prism 10.2.3	Dotmatics	RRID:SCR_002798